Dust Devil Tracks

Journal Item

Dust Devil Tracks

Dennis Reiss
Institut für Planetologie, Westfälische Wilhelms-Universität, Wilhelm-Klemm-Str. 10, 48149 Münster, Germany
phone: +49-251- 8339068
fax: +49-251- 8336301
dennis.reiss@uni-muenster.de

Lori Fenton
SETI Institute, 189 Bernardo Ave. Suite 100, Mountain View, CA, 94043, USA
lfenton@seti.org

Lynn Neakrase
Department of Astronomy, New Mexico State University, Las Cruces, NM, USA
lneakras@nmsu.edu

Michael Zimmerman
The Johns Hopkins University Applied Physics Laboratory, Laurel, MD, USA
Michael.Zimmerman@jhuapl.edu

Thiago Statella
Instituto Federal de Educação, Ciência e Tecnologia de Mato Grosso – IFMT, Brazil
thiago.statella@cba.ifmt.edu.br

Patrick Whelley
NASA Goddard Space Flight Center, Greenbelt, MD, USA
patrick.l.whelley@nasa.gov

Angelo Pio Rossi
Department of Earth and Space Sciences, Jacobs University Bremen, Bremen, Germany
an.rossi@jacobs-university.de

Matthew Balme
Department of Physical Science, The Open University, Milton Keynes, UK
Matt.Balme@open.ac.uk

Abstract

Dust devils that leave dark- or light-toned tracks are common on Mars and they can also be found on the Earth's surface. Dust devil tracks (hereinafter DDTs) are ephemeral surface features with mostly sub-annual lifetimes. Regarding their size, DDT widths can range between ~1 m and ~1 km, depending on the diameter of dust devil that created the track, and DDT lengths are range from a few tens of meters to several kilometers, limited by the duration and horizontal ground speed of dust devils. DDTs can be classified into three main types based on their morphology and albedo in contrast to their surroundings; all are found on both planets: (a) dark continuous DDTs, (b) dark cycloidal DDTs, and (c) bright DDTs. Dark continuous DDTs are the most common type on Mars. They are characterized by their relatively homogenous and continuous low albedo surface tracks. Based on terrestrial and martian in situ studies, these DDTs most likely form when surficial dust layers are removed to expose larger-grained substrate material (coarse sands of ≥ 500 µm in diameter). The exposure of larger-grained materials changes the photometric properties of the surface by leads resulting in lower albedo tracks because grain size is photometrically inversely proportional to the surface reflectance. However, although not observed so far, compositional differences (i.e., color differences) might also lead to albedo contrasts when dust is removed to expose substrate materials with mineralogical differences. For dark continuous DDTs, albedo drop measurements are around 2.5% in the wavelength range of 550 – 850 nm on Mars and around 0.5% in the wavelength range from 300 – 1100 nm on Earth. The removal of an equivalent layer thickness around 1 µm is sufficient for the formation of visible dark continuous DDTs on Mars and Earth. The next type of DDTs, dark cycloidal DDTs, are characterized by their low albedo pattern of overlapping scallops. Terrestrial in situ studies imply that they are formed when sand-sized material that is eroded from the outer vortex area of a dust devil is redeposited in annular patterns in the central vortex region. This type of DDT can also be found in on Mars in orbital image data, and although in situ studies are

lacking, terrestrial analog studies, laboratory work, and numerical modeling suggest they have the same formation mechanism as those on Earth. Finally, bright DDTs are characterized by their continuous track pattern and high albedo compared to their undisturbed surroundings. They are found on both planets, but to date they have only been analyzed in situ on Earth. Here, the destruction of aggregates of dust, silt and sand by dust devils leads to smooth surfaces in contrast to the undisturbed rough surfaces surrounding the track. The resulting change in photometric properties occurs because the smoother surfaces have a higher reflectance compared to the surrounding rough surface, leading to bright DDTs. On Mars, the destruction of surficial dust-aggregates may also lead to bright DDTs. However, higher reflective surfaces may be produced by other formation mechanisms, such as dust compaction by passing dust devils, as this may also cause changes in photometric properties. On Mars, DDTs in general are found at all elevations and on a global scale, except on the permanent polar caps. DDT maximum areal densities occur during spring and summer in both hemispheres produced by an increase in dust devil activity caused by maximum insolation. Regionally, dust devil densities vary spatially likely controlled by changes in dust cover thicknesses and substrate materials. This variability makes it difficult to infer dust devil activity from DDT frequencies. Furthermore, only a fraction of dust devils leave tracks, which also seems to vary regionally. However, DDTs can be used as proxies for dust devil lifetimes and wind directions and speeds, and they can also be used to predict lander or rover solar panel clearing events. Overall, the high DDT frequency in many areas on Mars leads to drastic albedo changes that affect large-scale weather patterns.

1. Introduction

Dust devil tracks (DDTs) are dark or bright surface lineaments left by passages of dust devils. Before dust devils had ever been detected on Mars, they were hypothesized to exist (Ryan 1964; Neubauer 1966; Sagan et al. 1971; Gierasch and Goody 1973). For a complete historical review about dust devils we refer here to Lorenz et al. 2016). The first direct observations of dust devils in Viking Orbiter images were made by Thomas and Gierasch (1985). For general information about orbital observations of dust devils we refer here to Fenton et al. (2016). Indirectly, Ryan and Lucich (1983) detected dust devils by their analysis of meteorological data acquired by Viking Lander 2 (see also Lorenz and Jackson 2016). Dark filamentary lineaments on the martian surface - which would nowadays be referred to as dust devil tracks (DDTs) - have already been visible in Mariner 9 images (Sagan et al. 1972; 1973; Cutts and Smith 1973; Veverka, 1975;1976). These observed albedo patterns were termed variable features (Sagan et al. 1972) because their size, shape and position were observed to change, which was correctly attributed to active aeolian processes on Mars. Most of these albedo features correspond with either albedo changes caused by a global-scale dust storm in 1971, or wind streaks with lifetimes lasting from seasons to decades (Malin and Edgett 2001). For further detailed classifications and summaries of variable albedo features on Mars, we refer the reader to Thomas et al. (1981) and Greeley and Iversen (1985). However, dark lineaments found on the floor of Proctor Crater (Figure 1A) were not described (Sagan et al., 1972) or these and other patterns of dark filamentary lineaments found elsewhere on Mars were either interpreted as linear seif dunes (Cutts and Smith 1973) or interpreted to be formed due to topographically controlled joints where strong winds are able to erode or deposit surface material (Veverka 1976).

Grant and Schultz (1987) first interpreted the dark, ephemeral, filamentary lineaments on Mars as features formed during the passage of ‘tornado-like vortices’. They linked the surface lineaments to local, ephemeral, and intense atmospheric phenomena because of the absence of structural or topographic control, gaps in lineaments, their non-destructive nature, seasonal occurrence, ephemeral nature, and year-to-year variation in distribution (Figure 1). They favored tornadic-intensity vortices caused by baroclinic wave passage through an area of atmospheric instability triggering convective uplift and strong shear, although they discussed and did not preclude their formation by dust devils. Based on terrestrial studies, Grant and Schultz (1987) found it unlikely that dust devils could cross large topographic obstacles and can leave such long and wide surface lineaments (up to 75 km long and 1 km wide), which would imply very large dust devils with very long durations. The development of the albedo difference between the dark surface lineaments to their surroundings was attributed by Grant and Schultz (1987) to the redistribution of coarser material into a narrow band (appearing darker due to coarse grained material versus finer grainer material in the surroundings), as an analogue to observed tornado tracks on Earth.

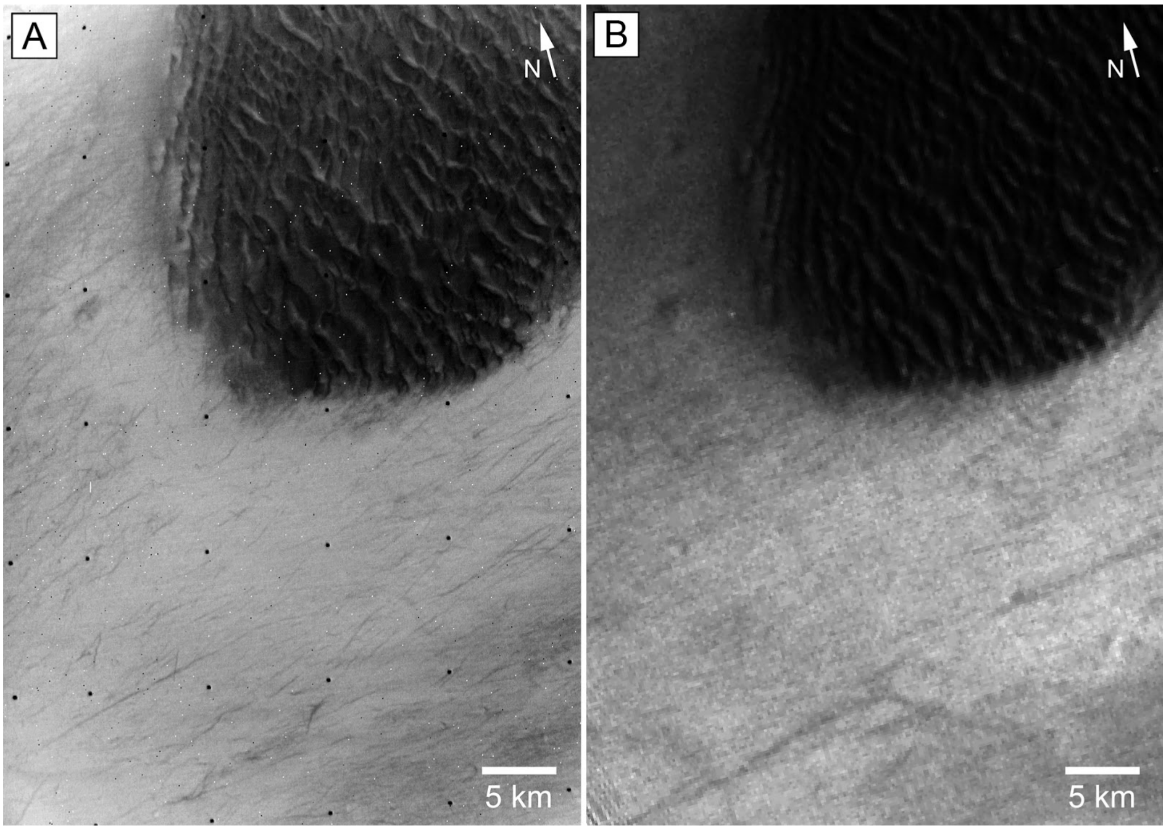

Figure 1. First observations of dark, ephemeral tracks (later found to be dust devil tracks; DDTs) on Mars in Proctor crater at 29.5°E and 48°S. (A) Example of dark filamentary lineaments in Mariner 9 images described by Veverka (1976). Mariner 9 image R229/09807499 acquired on 1972-03-07 with an image resolution of ~65 m/pxl. (B) Viking image F510A46 acquired on 1977-11-09 with an image resolution of ~175 m/pxl. The changes of dark lineaments to the Mariner 9 image (A) were mapped by Grant and Schultz (1987) (see Figure 3 in Grant and Schultz (1987)) and interpreted as ephemeral tornado-like tracks (Grant and Schultz, 1987).

About two decades after the end of the two Viking Orbiter missions, the Mars Orbiter Camera (MOC) onboard the Mars Global Surveyor (MGS) orbiter revealed that some of the dark lineaments (especially the larger ones) in Proctor crater interpreted by Grant and Schultz (1987) as DDTs are permanent features caused by boundaries between differing surface textures (Malin and Edgett 2001). However, the camera provided the first direct evidence of dust devils creating surface tracks (Edgett and Malin 2000). High-resolution orbital images acquired by the Mars Orbiter Camera–Near Angle (MOC-NA) instrument showed numerous active dust devils in the process of creating tracks (Edgett and Malin 2000; Malin and Edgett 2001; Cantor et al., 2006) (Figure 2). Additionally, the high-resolution capability of the MOC-NA (as fine as1.4 m/pixel) revealed the existence of not only dark (Figure 2A) but also bright DDTs (Figure 2B) on Mars (Edgett and Malin 2000; Malin and Edgett 2001). Furthermore, variations in dark DDT morphologies were detected, showing both dark continuous DDTs (Figure 2A) and dark cycloidal DDTs (Figure 2C) (Edgett and Malin 2000; Malin and Edgett 2001).

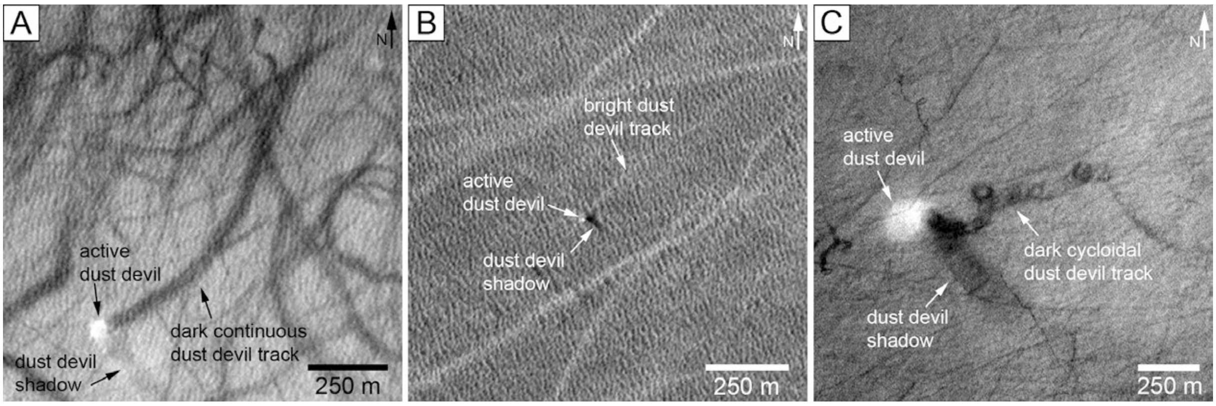

Figure 2. First direct observations that surface lineaments on Mars are created by passing dust devils. (A) Active dust devil with a dark continuous track resembling some of the dark filamentary tracks observed in Mariner 9 and Viking Orbiter images (MOC-NA image M1103289 in Hellas basin at 59.2°S and 22.1°E). (B) MOC-NA images also revealed that bright dust devil tracks (MOC-NA image S0501277 in Syria Planum at 14.9°S and 250.9°E) and (C) cycloidal patterns of dust devil tracks exist on Mars (MOC-NA image M1001267 in Promethei Terra at 54.1°S and 117.2°E).

Dust devil tracks on Earth were discovered relatively recently, largely due to the limited general availability of high spatial (and temporal) resolution imagery. The first known observation of DDTs on Earth was reported by Louis Maher who imaged bright DDTs from a lightplane occurring on dunes from in Sheep Springs, New Mexico, USA on 23 August 1959 (Figure 3A). This image was not published and is only available in the internet, but a general summary of the geology by lightplane roundtrip is given in Maher (1968). The first report of DDTs detected on satellite data dates back to 2002 (Rossi and Marinangeli 2004). These dark DDTs occur in the Ténéré desert (Niger) (Figure 3B) and have been observed over several years in ASTER data (Rossi and Marinangeli 2004). Mostly low-sinuosity tracks occur on diverse terrains: transverse dune fields, sand sheets and interdune seif zones (Rossi and Marinangeli 2004). The highest concentration of tracks could be observed on smooth interdunes and sand sheets. Their formation seems to have some seasonal dependency, with the largest number and surface density of tracks observed during spring (Rossi and Marinangeli, 2004; Reiss and Rossi, 2011).

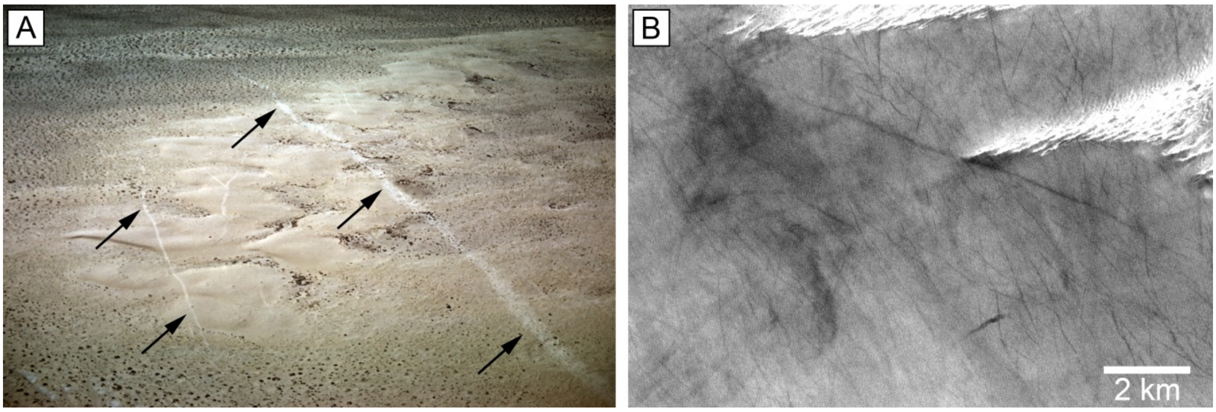

Figure 3. (A) Aerial image from a lightplane of bright dust devil tracks on dunes east of Chaco River , about 25 km northeast of Sheep Springs, NM, USA. View to SSW. (Image #052-21, 23 August 1959, Image credit: Louis J. Maher, Jr., http://geoscience.wisc.edu/~maher/air/air00.htm; ftp.geology.wisc.edu/maher/air). (B) Dark DDTs in the Ténéré desert (Niger) at 10.5°W and 18.85°N observed in an ASTER satellite image acquired on 26 May 2001 (Rossi and Marinangeli 2004).

During the following decade several more occurrences elsewhere were documented (Neakrase et al. 2008; 2012a; 2012b; Reiss et al. 2010; 2011a; 2013; Hesse, 2012). Overall, the number of detections is extremely low compared to those on Mars, where DDTs are rather ubiquitous. The physiographic, geologic, and geomorphologic setting of the areas where DDTs have been discovered and studied is somewhat variable, but all documented DDT discoveries share a climatic setting characterized by semi-arid to hyper-arid conditions (Figure 4).

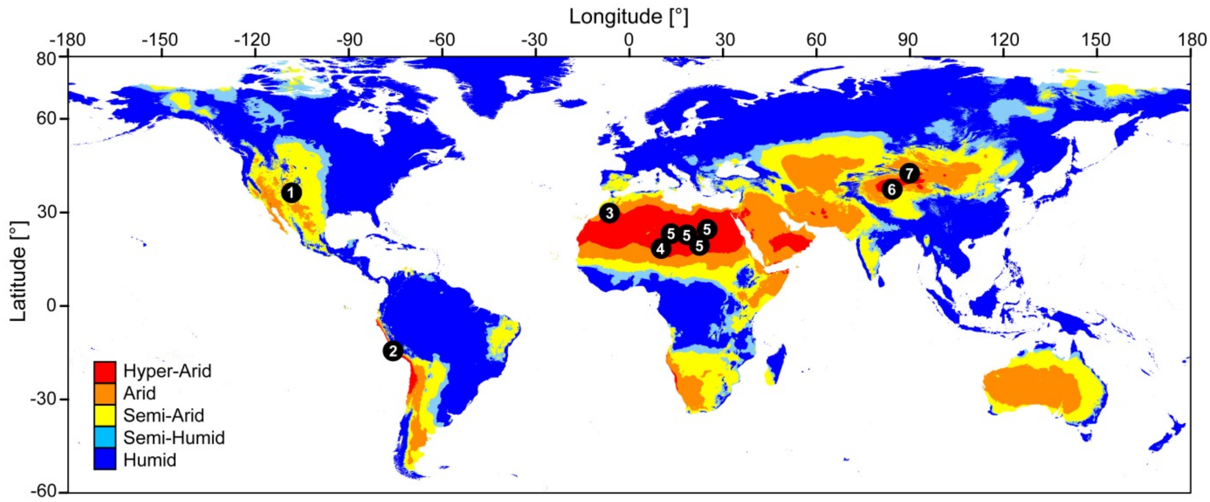

Figure 4. Global distribution of reported DDTs on Earth. (1) Maher (1968); (2) Hesse (2012), Reiss et al. (2013); (3) Reiss et al. (2012a, 2012b); (4) Rossi and Marinangeli (2004); (5) Neakrase et al. (2008, 2012); (6) Reiss (2016); (7) Reiss et al. (2010, 2011). Background: Humid to Hyper-Arid climate zones from CGIAR-CSI Global-Aridity database (http://www.cgiar-csi.org; Zomer et al. 2007; 2008).

In this review paper, we summarize the current knowledge about DDTs on Mars and Earth. The paper is structured as follows: In section 2. we classify DDTs by their morphology and albedo contrast to their surroundings, and for each DDT type we present possible formation mechanisms for both planets. In addition, in this section we give further information about each DDT type, such as lifetimes, if available. In section 3, we present the spatial and temporal DDT distribution on Mars. In section 4, we present how DDTs can be used as proxies for dust devil activity, dust devil minimum durations, ambient wind directions, surface wind conditions, and predictions for landed spacecraft solar panel clearing events. Then, section 5 highlights global albedo changes caused by DDTs and how these changes impact the climate system of Mars. In section 6, we present recent advances in detecting DDTs automatically in satellite imagery from Mars. Finally, in section 7 we summarize the paper and concurrently identify knowledge gaps and point out future directions in DDT research.

2. Morphology, Classification and Formation

In plan view, DDTs generally show linear, curvilinear, curved, meandering or looping streak morphologies (Figure 5A and B). They might be confused with other low albedo features such as wind streaks (Balme et al. 2003). However, DDTs are typically singular, not completely straight and crisscross other tracks, whereas streaks formed by wind gusts exhibit multiple straight parallel to subparallel lineaments (Figure 5C) (Cantor et al. 2006). Regarding their size, most DDTs have relatively constant widths. On Mars, they generally range from 10 m to 200 m in width and up to a few kilometers in length (e.g., Balme and Greeley 2006; Fisher et al. 2005, Verba et al. 2010). One might expect DDT width distribution would resemble that of dust devils, because small dust devils occur more often than larger ones (Sinclair, 1969; Carroll and Ryan, 1970; Snow and McClelland, 1990; Pathare et al, 2010; Greeley et al., 2010; Lorenz, 2011). However, reported observations of DDT widths seem to be biased towards wider dust devils, which might be because DDTs mainly form as a result of more intense, large dust devils, because certain surface properties only enable DDT formation from the larger dust devils, and/or because the DDT images that have been analyzed have low spatial resolution and thus do not capture the smaller DDTs. Interestingly, in some regions DDT widths observed in high resolution HiRISE images seem to be exclusively dominated by small DDTs between 1 and 10 m in width and 100 meters to few kilometers in length, which is possibly related to a low thickness of the Planetary Boundary Layer (PBL) in these regions suppressing larger dust devil size populations (Reiss and Lorenz 2016). In general, observed DDT sizes on Earth tend to be narrower than martian DDTs, with dimensions ranging generally from 1 to a few 10s of meters in width and between a few 100s of meters to several kilometers in length (Rossi and Marinangeli 2004; Hesse 2012; Reiss et al. 2010; 2011a; 2013). The observation that terrestrial DDTs are narrower than their martian counterparts may reflect the smaller dust devil size population on Earth relative to Mars (Fenton et al., 2016).

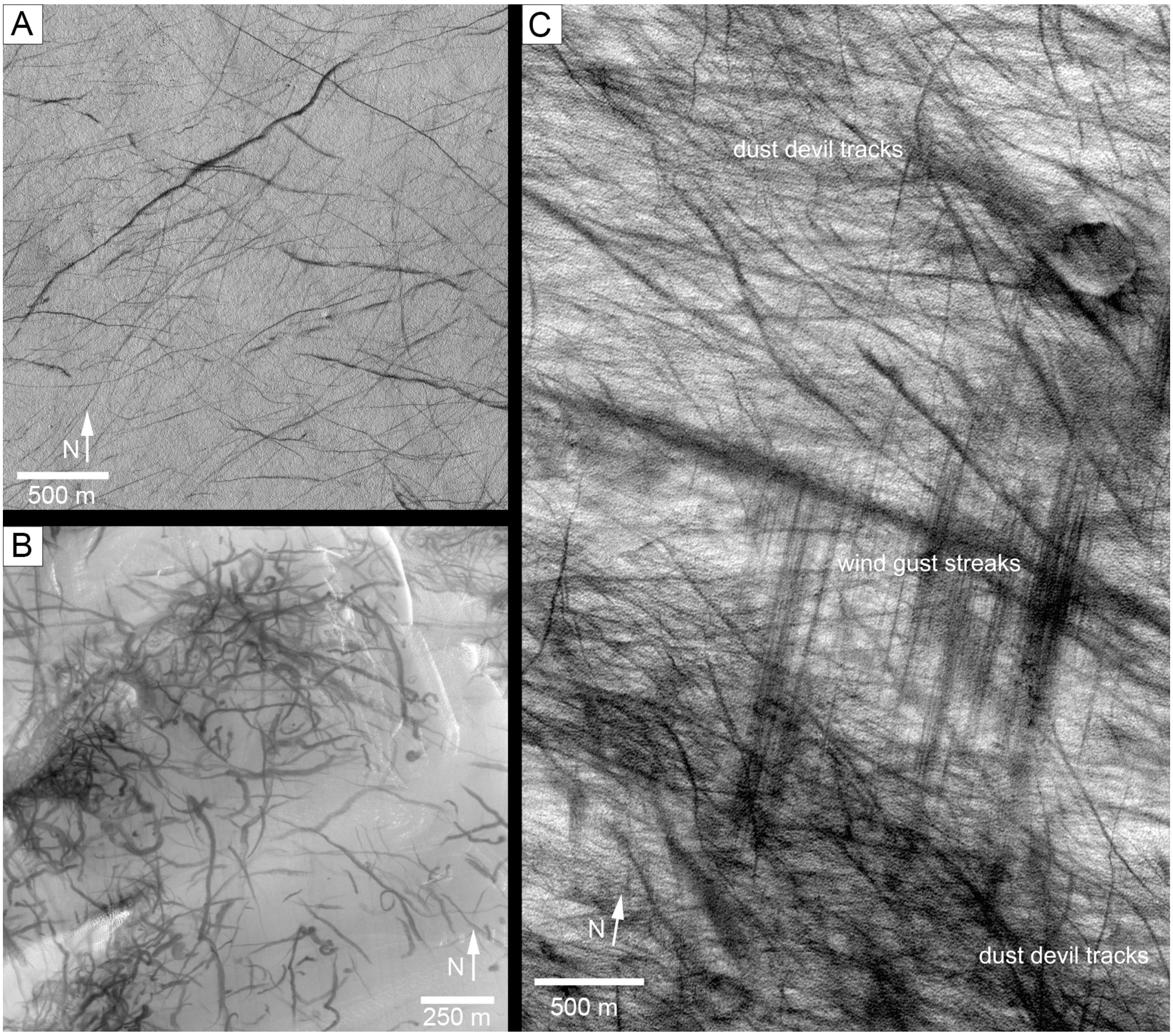

Figure 5. (A) Linear to curvilinear DDTs in the Thyles Rupes region at 68.53°S and 145.02°E (HiRISE image ESP_013751_1115). (B) Curved, meandering and looping DDTs on the Russell crater dune field at 54.27°S and 12.95°E (HiRISE image PSP_005383_1255). (C) Wind gust streaks and DDTs in Malea Planum at 67.15°S and 43.9°E (MOC-NA image R1103946). The wind gust streaks shown are linear, aligned in a parallel pattern in the north-south direction, whereas the DDTs are linear to curvilinear, aligned mostly in a west-east direction. See also Cantor et al. (2006).

DDTs on Earth and Mars can broadly be classified into three categories based on their morphology and the albedo contrast relative to their surroundings. Most DDTs are dark compared to their surroundings, but they can differ in morphology, exhibiting either continuous dark lineaments or discontinuous dark cycloidal patterned surface streaks. More rarely, relatively bright lineated tracks occur. Martian examples of each of these three DDT categories are shown in Figure 2 and each of these categories have also been found on Earth. In the following section, we classify and present the current knowledge about the individual DDT types.

2.1 Dark Continuous DDTs

One of the most common low albedo lineaments on the martian surface are dark continuous DDTs. They are characterized by their relatively homogenous and continuous low albedo surface track pattern in contrast to dark cycloidal patterned DDTs (see section 2.3). Figure 6 shows two examples from Gusev crater, one obtained from orbit by the HiRISE camera and one from the martian surface by the Navcam camera onboard MER-A (Spirit) rover.

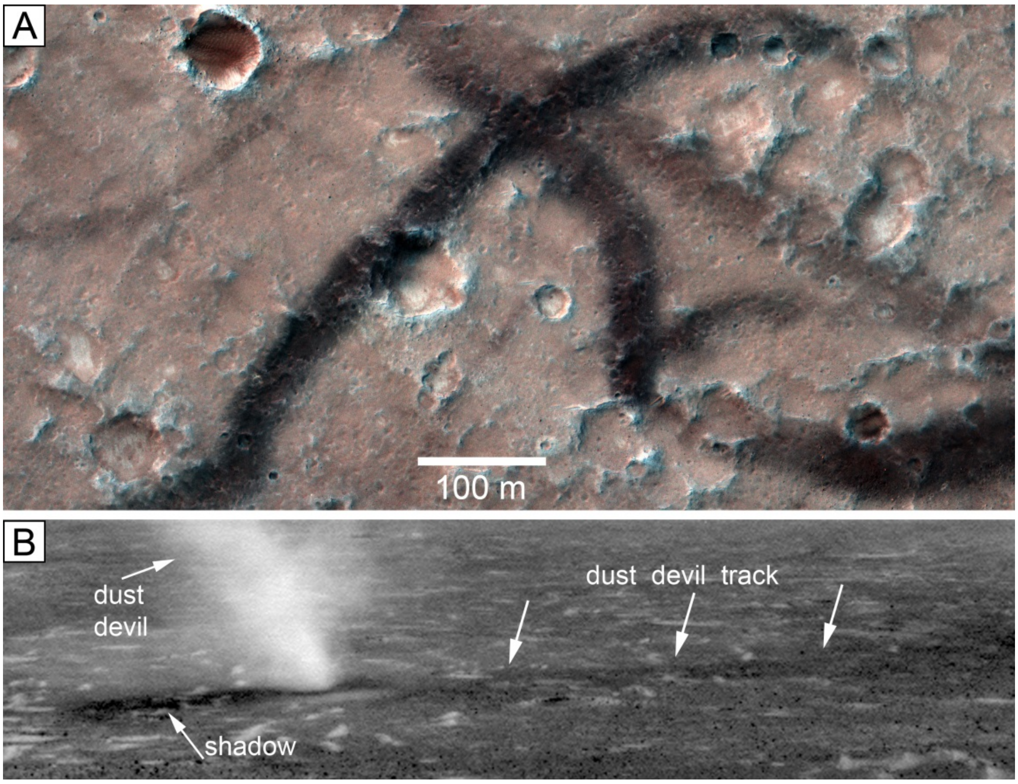

Figure 6. (A) High-resolution orbital view of dark continuous DDTs in Gusev crater at 14.6°S and 175.5°E (HiRISE IRB-image PSP_006524_1650 with a spatial resolution of 25 cm/pxl). (B) Active dust devil (diameter of ~100 m) in Gusev crater moving from right to left leaving a dark continuous DDT in its wake (MER-A (Spirit) Navcam image 2n176788730radadaep1560l0c1). For the full image sequence see also Greeley et al. (2010).

The formation of dark continuous DDTs is suggested to be linked to the removal of a surficial dust layer by passing dust devils and their fading with time due to subsequent airfall dust deposition (e.g., Malin and Edgett, 2001; Balme et al., 2003). The albedo contrast between dark continuous DDTs and their surroundings might be explained by compositional differences or photometric differences between the eroded dust and exposed surface material. Airfall dust on the surface of Mars is similar in composition to the global soil and basaltic crust, but it is enriched in S, Cl, and Fe (e.g., Rieder et al. 1997; Goetz et al. 2005; Yen et al. 2005; Berger et al. 2016). The removal of surface dust by dust devils likely exposes soils with a different composition, which might result in the formation of DDTs. However, photometric effects due to changes of grain size might be a more common cause of albedo differences because the reflectance depends on particle size. Larger grains have greater internal photon path lengths which increases absorption, whereas smaller grains have proportionally more surface reflections that shorten internal photon path lengths (e.g., Hapke 1981; Hapke 1993; Clark and Roush, 1984). The surface-to-volume ratio is a function of grain size and as a consequence the reflectance decreases with increasing grain size in the visible and near-infrared wavelengths. The effect that changing a surface's grain size has on its photometric properties was studied by Wells et al. (1984), who used Mars-analog materials of Mauna Kea volcanic soil to conduct reflectance measurements of varying amounts of deposited dust particles (1 – 5 µm in diameter) on a larger-grained substrate (< 44 – 250 µm in diameter) at visible and near-infrared wavelengths (0.4 – 1.2 µm). Their laboratory experiments showed that the spectral and photometric properties of the substrate material are significantly affected even after deposition of very small amounts of dust particles (Figure 7). Conversely, the erosion of fine dust particles from a coarser grained substrate such as sand would lead to a decreased reflective surface, hence leading to a darker surface area in the wake of passing dust devils.

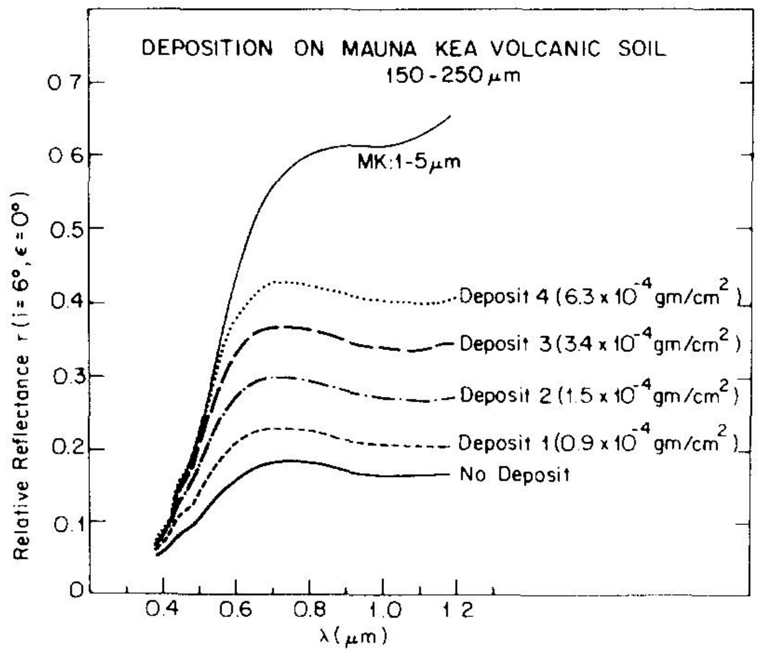

Figure 7. Reflectance changes of 150 – 250 µm particles (Mauna Kea volcanic soil) after progressive deposition of 1 – 5 µm particle sizes (from Wells et al. 1984). **PERMISSION**

The MER-A (Spirit) rover landed in Gusev crater within an area exhibiting various aeolian features, including seasonal dust devil activity and DDT formation (Greeley et al. 2005; Greeley et al. 2006a; Figure 6). The Spirit rover crossed a dark continuous DDT (Greeley et al. 2005), making it possible to investigate the surface substrate inside and outside the track with the Microscopic Imager (MI) (Herkenhoff et al. 2003). These in situ studies revealed that the surface substrate within the dark DDT area, consisting of coarse sand (500 – 1000 µm), was relatively free of the fine grained dust (Figure 8A) compared to the brighter regions outside the track (Figure 8B) (Greeley et al., 2005). This implies dust devils surficially remove dust, leading to photometric changes within the DDT area (Figure 8A). Specifically, the albedo difference between the DDT and its surroundings can be explained by the removal of a thin dust layer leading to the exposure of coarse sand grains within the track area; hence, the reflectance in the visible and near-infrared wavelengths within the track area decreases in comparison to the surroundings, which are still dust covered, because brightness is photometrically inversely proportional to grain size (Greeley et al. 2005). In Figure 8A, the texture of the surface consisting of coarse sands within the track area is still indicative of a thin layer of dust material coating the coarse sand, even after surficial dust removal exposing the coarse sand by the passing dust devil. This indicates that for this DDT, compositional effects did not or only minorly contribute to its formation. However, this is the only in situ study of a martian DDT to date, such that compositional differences producing dark continuous DDTs might be relevant elsewhere on Mars.

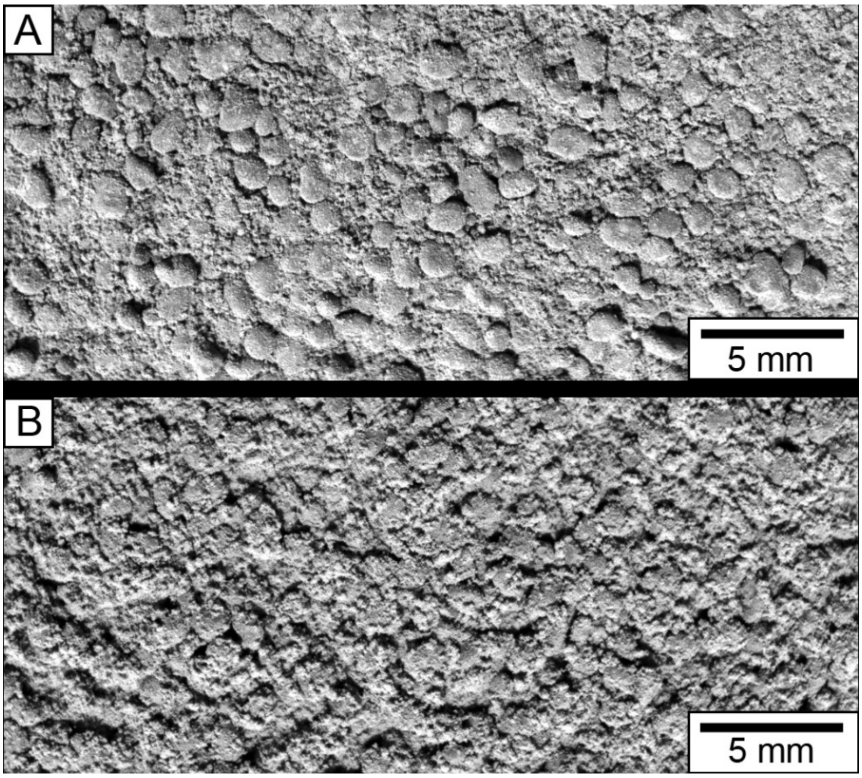

Figure 8. Microscopic images (A) inside (MI image 2m129820106cfd0400p2943m2f1) and (B) outside of a DDT (MI image 2m132840805cfd2000p2937m2f1) in Gusev crater (see also Greeley et al. 2005). (A) Exposed coarse sand within the DDT, which is relatively free of fine dust compared to (B) outside the DDT. Note that the spatial image resolution of the MI is not able to resolve single dust grains, but the texture is indicative of fine dust coating coarse sand grains.

How much dust needs to be eroded for DDTs to form? In most cases, the amount of eroded dust from the surface is given in an equivalent layer thickness not including pore space between the dust grains. This dust deflation produced by dust devils creating DDTs was estimated to be in the range of a few to several tenths of microns (Malin and Edgett, 2001; Balme et al., 2003). Direct measurements from rover imaging instruments such as the MI are difficult because the instrument is not able to spatially resolve dust grains (see also Figure 8). However, the removed thickness of a dust layer can be inferred indirectly from active dust devils leaving tracks using observed characteristics of their behavior, although there exist relatively large uncertainties associated with such obtained dust fluxes. In the following dust deflation estimates from lander, orbital and large-eddy simulations (LES) are presented.

Figure 6B shows an active dust devil in Gusev crater, leaving a track in its wake, captured in time-sequential images acquired by the Navcam onboard the MER rover Spirit (Greeley et al. 2010). From the sequential images, Greeley et al. (2010) were able to estimate the vertical speed within the dust devil and its dust load, calculating a dust flux of 1.6×10^{-5} kg m^{-2} s^{-1}. They also approximated the diameter of the dust devil to be ~100 m and the horizontal ground speed to be 4.4 m s^{-1} (Greeley et al. 2010). Using the estimated value of the dust flux, and the measured diameter and horizontal ground speed, it is possible to calculate the eroded dust layer because it is known how long the dust devil stayed above a specific point on the surface (Metzger, 1999). In the case of the dust devil in Figure 6B, which is leaving a track in Gusev crater, the dust devil needed about 23 s to cross a given spot on the surface; this translates into an eroded dust equivalent thickness layer of ~1.5 μm using a dust grain density of 3000 kg m^{-3}.

A similar method was used by Reiss et al. (2014b) but estimating the eroded dust thickness from orbital images and assuming typical vertical speeds within vortices., The diameters, dust loads, and horizontal ground speeds of two active dust devils leaving tracks were measured from orbital imagery. Using the range of typical vertical speeds found in dust devil cores (0.1-10 m s^{-1}) as measured on both Earth and Mars (Ryan and Carroll 1970; Fitzjarrald 1973; Sinclair 1966; Sinclair 1973; Metzger 1999; Metzger et al., 2011; Greeley et al. 2006b; Greeley et al. 2010) the minimum and maximum dust fluxes can be calculated. In combination with the measured dust devil diameter and the horizontal ground speed, the dust deflation can then be calculated. The maximum eroded dust equivalent thickness layer of both dust devils leaving tracks was < ~2 µm using a dust grain density of 3000 kg m^{-3} (Reiss et al. 2014b).

Along with direct observations, dust deflation can also be calculated using large-eddy simulations (LES). Numerical calculation of DDT formation by Michaels (2006) using the Mars Regional Atmospheric Modeling System (MRAMS) produced an eroded dust equivalent thickness layer ranging from ~1 – 8 µm within the track area (Figure 9). However, in the majority of the track area the eroded equivalent thickness layer was less than 1.5 µm (Michaels 2006) which is consistent with calculated values from direct observations on Mars (e.g., Reiss et al. 2014b). The average diameter of airborne dust particles on Mars is around 3 µm (Pollack et al.1995; Tomasko et al. 1999; Markiewicz et al. 1999; Lemmon et al. 2004; Wolff et al. 2006), hence the erosion of less or about one monolayer of surficial dust can be sufficient to form dark continuous DDTs.

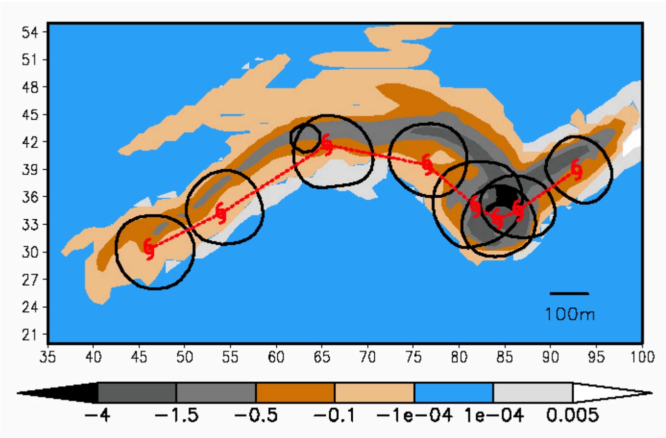

Figure 9. Numerical simulation of DDT formation on Mars (from Michaels 2006). Colors indicate the depth of net surface dust reservoir change in µm (negative values = dust removal). The red line indicates the position of the vortex center, and black contours indicate the extent of the vortex core walls (Michaels 2006). **PERMISSION**

Albedo measurements between DDTs and their surroundings are rare. Statella et al. (2015) calculated albedo contrasts between DDTs and their surroundings in 5 regions on Mars (Argyre, Aeolis, Eridania, Noachis, and Hellas) using HiRISE images with band passes between 550 and 850 nm. The mean albedo contrasts are between ~ 2 - 3 % ± ~1.5 %.

Observed lifetimes based on multi-temporal image coverage of dark continuous DDTs are relatively short, ranging from a few weeks to less than one martian year (e.g., Balme et al. 2003; Cantor et al. 2006; Greeley et al. 2010; Verba et al. 2010; Reiss and Lorenz 2016). DDTs are erased by the steady or seasonal settling of atmospheric dust (e.g., Balme et al. 2003; Cantor et al. 2006) or an increased dust deposition after dust storm events (Greeley et al., 2010; Verba et al., 2010; Reiss and Lorenz 2016). At higher latitudes, seasonal frost deposits can also lead to the erasure of DDTs (Cantor et al. 2006). These different short- to long-term erasure mechanisms likely explain the relatively broad range of DDT lifetimes.

Terrestrial in situ studies of dark continuous DDTs are rare. First observations of dark continuous DDTs were made by Rossi and Marinangeli (2004) on medium-resolution satellite images. Resembling martian DDTs, they were found to occur in the Ténéré desert (Niger). In the following years, several more detections of dark continuous DDTs in satellite images have been reported in the Saharan desert (Neakrase et al. 2008; 2012) and in the Turpan desert in northwestern China (Reiss et al. 2010) (Figure 10). Reiss et al (2010) analyzed dark continuous DDTs in the Turpan desert in northwestern China that were previously detected on high-resolution satellite imagery. Figure 10B shows an example of an active dust devil leaving a dark continuous track in its wake. The occurrence of dark continuous DDTs is limited to rippled surfaces consisting of coarse to very coarse sand grains (500 – 2000 µm) (Reiss et al., 2010; 2012). Microscopic images taken with a handheld device revealed that the sand substrates on the ripple surfaces are relatively free of fine-grained dust (< 63 µm) compared to the areas outside of the track area (Figure 11) (Reiss et al., 2010). This suggests that passing dust devils erode dust deposits located on top of the sandy surfaces, leading to photometric changes, hence darker surface areas (dark continuous DDTs) where the dust is removed. Dark continuous DDTs only occur on surfaces consisting of sand with grain sizes >500 µm, althoughmost of the Turpan desert area is covered by a large dune field consisting of fine sand (~125 µm), on which dark continuous DDTs were not observed to form (Reiss et al., 2010). This suggests that for photometric changes (rather than compositional changes) to result in DDTs, the grain size differences between the substrate material and the overlying dust needs to be sufficiently large. This terrestrial formation mechanism is in agreement with the formation of dark continuous DDTs on Mars.

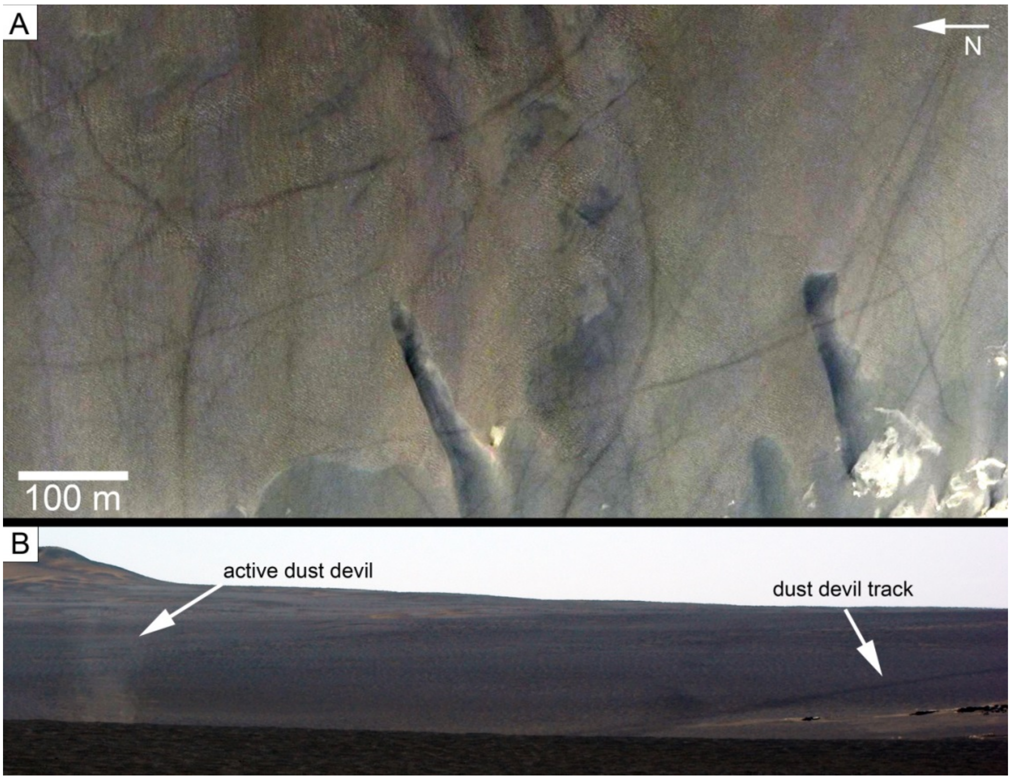

Figure 10. (A) High-resolution satellite image showing several dark continuous DDTs in the Turpan desert acquired on 03 April 2005 (Quickbird image with a resolution of 0.6 m/pxl accessed through Google Earth). (B) Example of an active dust devil (diameter ~3 m) in the Turpan desert leaving a dark continuous DDT on 20 April 2010. See also Reiss et al. (2010).

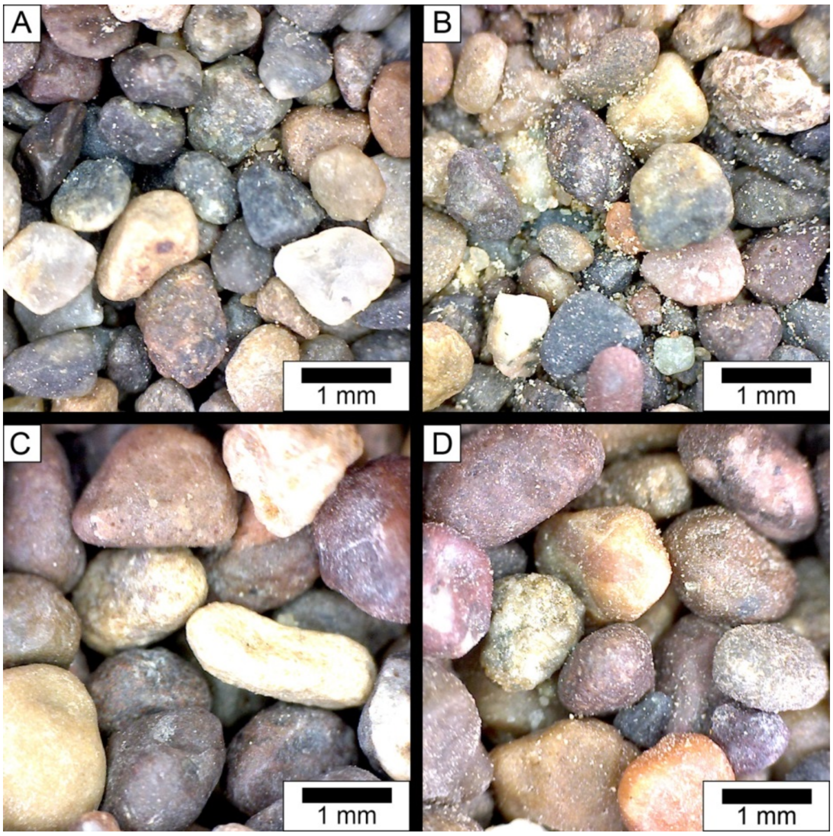

Figure 11. Microscopic imagery (magnification factor 20 x) within (A and C) and outside (B and D) of dark continuous DDT areas taken in the Turpan desert. A and B were taken on ripple surfaces, and C and D on large ripple surfaces. All photographs were taken on ripple crests. See also Reiss et al. (2010).

For the dark continuous DDTs analyzed from the Turpan desert, the removed equivalent dust layer thickness was estimated to be about 2 µm (Reiss et al., 2010), based on size measurements of dust particles in the obtained microscopic images (Figure 11). A subsequent study using a larger number of microscopic image data and refined techniques estimated the removed equivalent dust layer thickness to be about 1.2 µm (Reiss et al., 2012). These dust removal thicknesses are in the same range as those observed on Mars, indicating that the deflation of relatively thin dust layers are sufficient for the formation of dark continuous DDTs on both planets.

Reiss et al. (2012) measured albedo contrasts of two DDTs and their surroundings in the Turpan desert using a pyranometer in the visible wavelength range from 300 to 1100 nm. The dark continuous DDTs were ~0.5 and ~0.6% darker than the adjacent terrain.

Based on multi-temporal image coverage the lifetime of dark continuous DDTs in the Ténéré desert (Niger) is sub-annual (Rossi and Marinangeli 2004).

2.2 Bright DDTs

Bright DDTs resemble dark continuous DDTs but exhibit a higher albedo than the surrounding areas (Figure 12). On Mars, they are less common than dark ones (Edgett and Malin, 2000; Malin and Edgett 2001; Cantor et al. 2006), have lifetimes of less than five terrestrial months (Cantor et al. 2006), and seem to be confined to specific regions such as Amazonis Planitia, Syria Planum (Cantor et al. 2006) and Arsia Mons (Cushing et al. 2005). These regions are known to exhibit a relatively thick dust cover (Ruff and Christensen 2002) indicating that a sufficient amount of fine dust on the surface is required for their formation (Reiss 2014). However, comprehensive studies about the distribution or formation mechanisms of bright DDTs on Mars are lacking.

Whelley and Greeley (2008) suggested that bright DDTs on Mars might be formed by 1) removal of dark dust, 2) exposure of a bright underlying substrate, or 3) a compaction mechanism by the downdraft of dust devils. Hoffer and Greeley (2010) proposed a compaction mechanism based on laboratory experiments in which a reorientation of individual dust grains resulted in a closer packing and produced higher reflective surfaces due to changes in photometric properties. Based on terrestrial in situ studies (see the following section), Reiss et al. (2011a) proposed that bright DDTs on Mars might be formed due to the destruction of dust aggregates as passing dust devils leave a smoother, higher reflective surface within the track area in contrast to the rougher (at mm-scale), lower reflective track surrounding areas. Interestingly, MER rovers have observed weakly bound dust aggregates ≥100 µm to several mm in size (Vaughan et al. 2010)—held together by van der Waals, electrostatic, or other inter-particle forces—on the martian surface (e.g., Herkenhoff et al., 2004, 2006; Sullivan et al., 2008; Bridges et al., 2010).

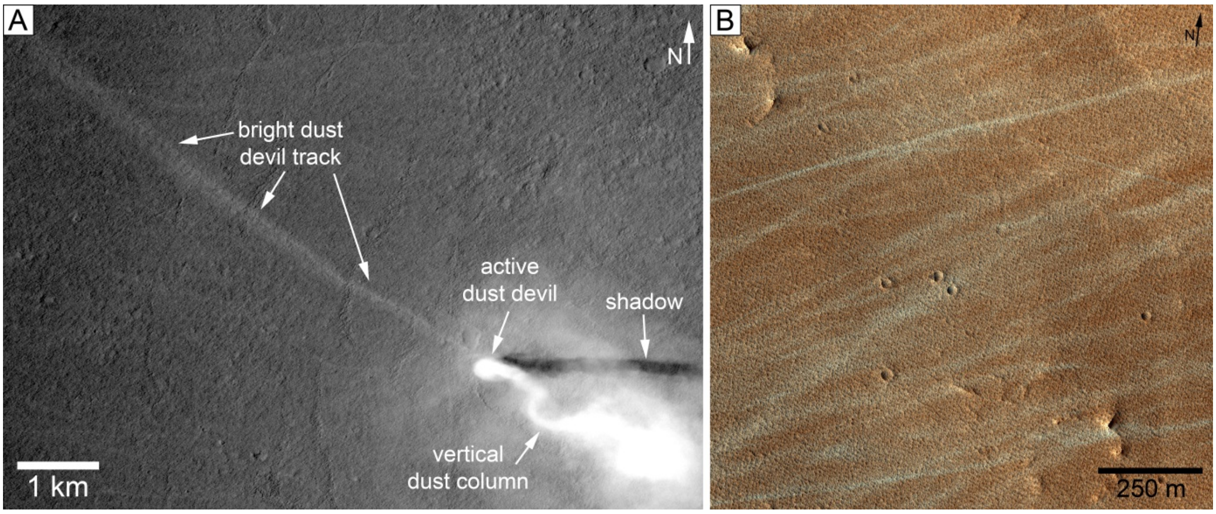

Figure 12. (A) Active dust devil in Amazonis Planitia leaving a bright DDT in its wake (CTX image G21_026394_2155_XN_35N158W at 34.9°N and 201.7°E). (B) Numerous bright DDTs in Syria Planum (HiRISE image PSP_005453_1680 at 11.7°S and 258°E).

On Earth, Maher (1968) suggested that bright DDTs (see also Figure 3A) are caused by the disturbance of desert varnish by passing dust devils. However, this mechanism is highly unlikely because active dust devils are not strong enough to disturb hard crusts, which normally need to be scratched. Reiss et al. (2011a) observed bright DDTs in the Turpan desert and made the first in situ studies. Usually, dark continuous DDTs occur in this area (see section 2.1), but after a rainfall event only bright DDTs were observed in the field (Reiss et al. 2011a) (Figure 13). Raindrop impacts onto the surface caused the formation of aggregates of sand, silt, and clay, leading to rough surface textures (Figure 13B). Due to their weak cohesion, passing dust devils easily destroyed the aggregates, leading to smooth surface textures at the millimeter scale (Figure 13C). The albedo difference between the track area and the surroundings can be explained simply by photometric effects between the smoother, higher reflective track area and the rougher (at mm-scale), lower reflective surroundings (Reiss et al. 2011a). Based on field observations, bright DDTs in the Turpan desert remained only for a few days likely due to the destruction of surficial aggregates by strong winds (Reiss et al. 2011a).

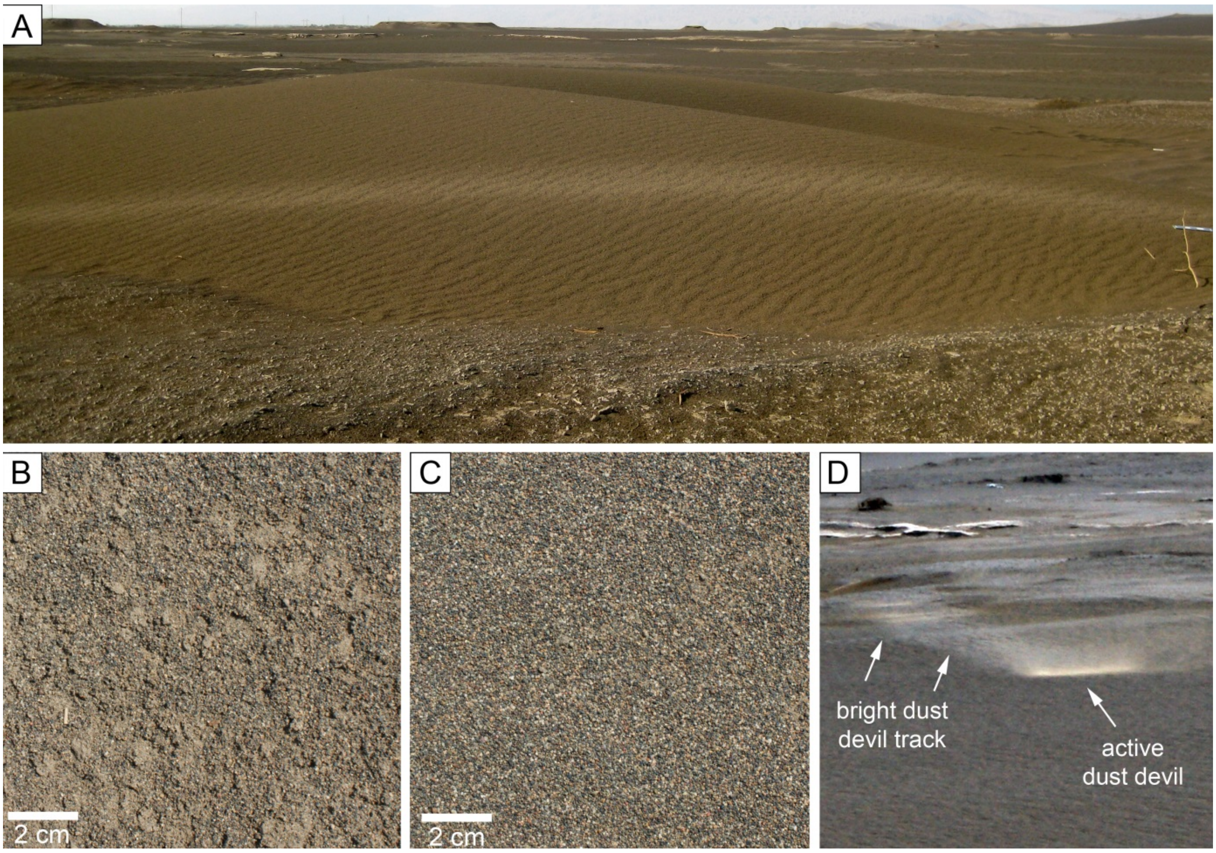

Figure 13. (A): Bright DDT (~1 m width) observed on a sand dune in the Turpan desert. (B) Rough surface texture due to soil aggregates caused by raindrop impacts outside the DDT. (C) Smooth surface texture within the DDT area, occurring after the dust devil destroyed the

aggregates. (D) Direct observation of an active dust devil leaving a bright track in its wake. Note that the dust column of the dust devil is faint, but the sand skirt near the ground is clearly visible. See also Reiss et al. (2011a).

2.3 Dark Cycloidal DDTs

Dark cycloidal DDTs were first observed in satellite imagery by Hesse (2012) in southern Peru. In plan view, they are characterized by a low albedo cycloidal pattern of overlapping scallops, sometimes accompanied by lateral bright margins on one or both track sides (Figure 14A). In comparison to dark continuous DDTs, the tracks of dark cycloidal DDTs are not continuously dark, but rather only the overlapping scallops show a low albedo, which forms the cycloidal track pattern. In morphology, the tracks resemble ground marks left by tornadoes (Figure 14B), which form their cycloidal pattern by depositing debris (including corn stubbles on farmland, etc.) gathered by suction vortices (e.g., van Tassel, 1955; Prosser, 1964; Fujita et al., 1970; Fujita, 1971; Fujita, 1974).

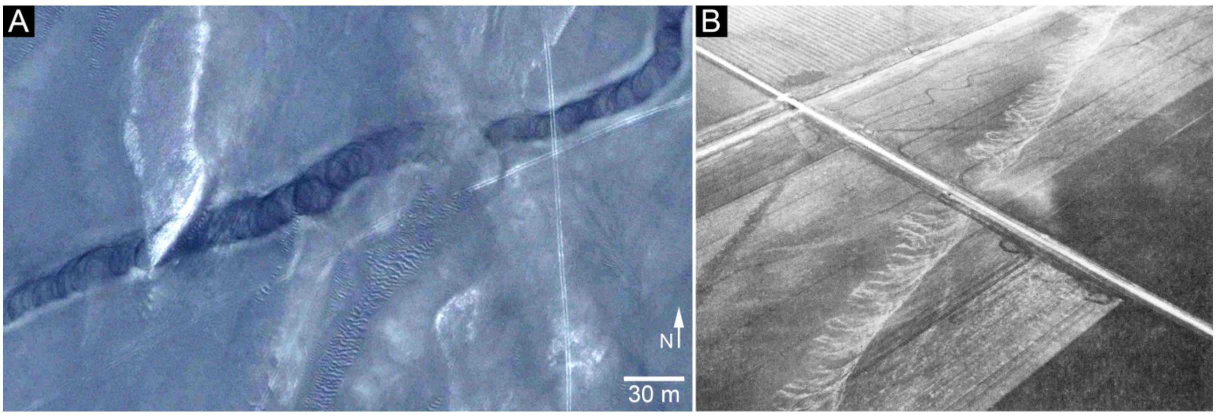

Figure 14. (A) Dark cycloidal DDT in southern Peru at 14.2°S and 75.9°W (DigitalGlobe satellite image accessed through Google Earth). (B) Cycloidal tornado track left by Anchor (No. 2) tornado of 3 April 1974 (Image credit: Fujita (1974) **PERMISSION Weatherwise**

from Davies-Jones (1986)). Note that the tornado track in (B) is bright due to the deposition of relatively bright corn stubbles.

Multi-temporal satellite images show that the lifetime of cycloidal DDTs in southern Peru can vary drastically. In some regions, dark cycloidal DDTs can still be identified after several years (long-lived) whereas in other regions they disappear within one year (short-lived) (see examples in Hesse (2012) and Reiss et al. (2013). In situ studies of short-lived and long-lived dark cycloidal DDTs in southern Peru revealed that cycloidal track patterns are formed by redeposition of sand-sized material, which is eroded by dust devils from the outer track margins and is subsequently deposited in annular patterns in the vortex cores (Reiss et al. 2013). Figures 15A and B show an example of long-lived cycloidal DDT in southern Peru with accompanying bright margins as seen from orbit and in the field, respectively. The long-lived cycloidal DDTs are located on a desert pavement surface consisting of a layer of crusted fine-material (< 250 µm) overlain by very coarse sand grains (1 – 2 mm) (Figure 15E). The bright marginal area of the track shows a reduced fraction of very coarse sand grains (Figure 15D) compared to the undisturbed desert pavement surface (Figure 15E). In contrast, there is an increased fraction of very coarse sand grains within the dark cycloidal DDT area (Figure 15C) relative to the undisturbed desert pavement surface (Figure 15E). This implies erosion of the surficial very coarse sand at the outer margins of vortices (leaving deflated bright margins) and their subsequent deposition in annular patterns within the vortices (forming the deposited cycloidal pattern) (Reiss et al. 2013). The albedo differences between the dark track, bright margins, and the surrounding area can be explained by changes in photometric properties caused by different amounts of surficial very coarse sand. The long lifetime of dark cycloidal DDTs in this area can simply be explained by their occurrence on desert pavements that do not experience much aeolian activity. Field experiments on desert pavements in other region on Earth showed that the recovery of relatively small areas cleared from stones and granules occurs at very low rates of about 1 % per year, which indicates full surface recovery times of up to 80 years (Haff and Werner, 1996).

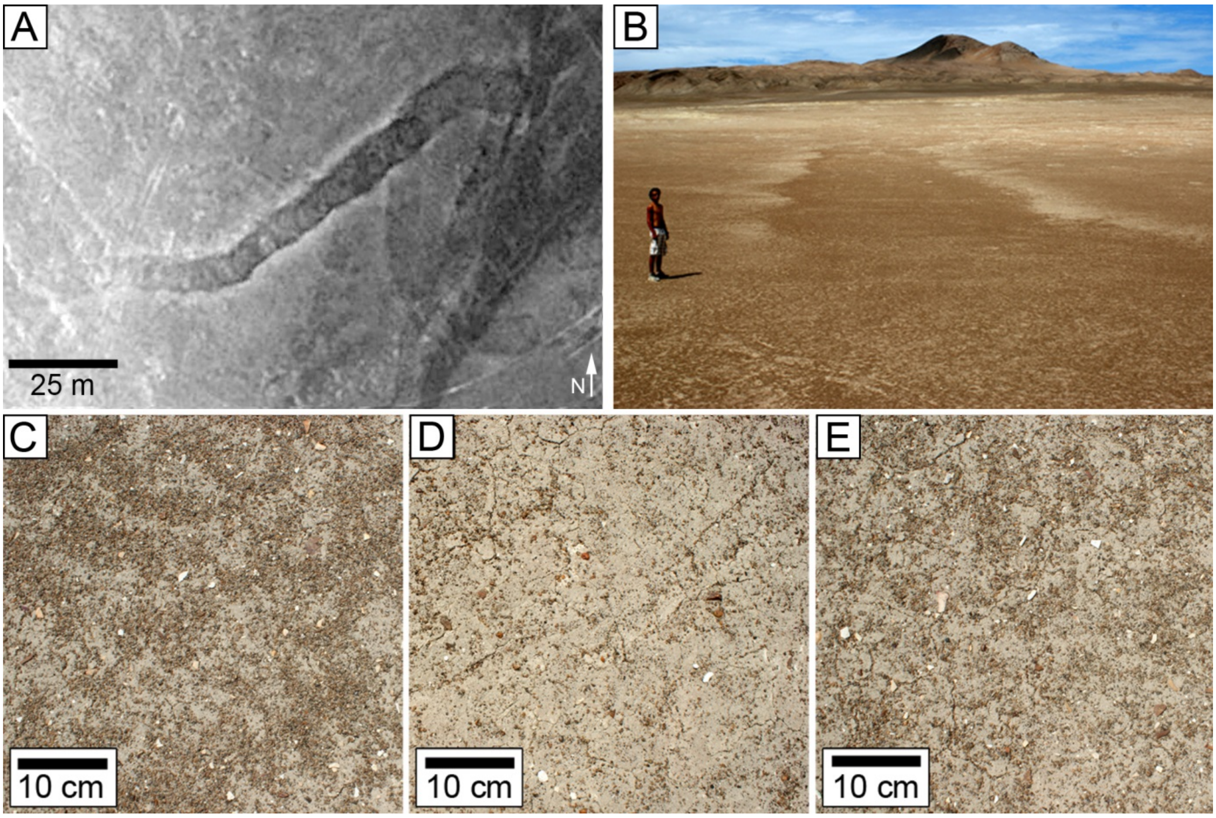

Figure 15. (A) Long-lived dark cycloidal DDT in southern Peru at 14.4°S and 75.8°W (DigitalGlobe satellite image accessed through Google Earth). (B) Field photograph of the same DDT as in A, imaged facing southwest. Note the bright margins of the dark track area. (C) Top-view image of the dark cycloidal track area. (D) Top-view image of the bright margin area. (E) Top-view image of an area outside the dark and bright margin area of the cycloidal track area. For further information see also Reiss et al. (2013).

Compared to long-lived dark cycloidal DDTs, such as those shown in Figure 15, short-lived dark cycloidal DDTs rarely have lateral bright margins. Examples of short-lived dark cycloidal DDTs in southern Peru are shown in Figure 16A, which occur on sand sheets consisting of granule ripples dominated by coarse to very coarse sand (0.5 – 2 mm). Ripple troughs are relatively free of coarse sand, and bright patches of the underlying fine grained material (< 250 µm) are visible (Figure 16B and C). In situ studies of the dark cycloidal DDT shown in Figure 16B by Reiss et al. (2013) revealed that the bright patches (Figure 16C) within the track area are covered by coarse sand (Figure 16D), indicating that active dust devils redistribute sand material in annular patterns within the track area leading to dark cycloidal DDTs. The rarer occurrence of bright marginal areas along the dark track of short-lived dark cycloidal DDTs can be explained by the large amount and thickness of coarse sand (in contrast to the desert pavement region where long-lived DDTs usually exhibit bright lateral areas) impeding complete exposure of the bright underlying surface by erosion. However, some dust devils seem to be strong enough to remove enough sand to create bright marginal areas along one (Figure 16A, arrow 2) or both sides (Figure 14A) of the dark cycloidal tracks. The relatively short lifetime of the DDTs on these surfaces can be explained by their occurrence on active aeolian sand sheets, which mobilize the coarse grains and destroy the tracks.

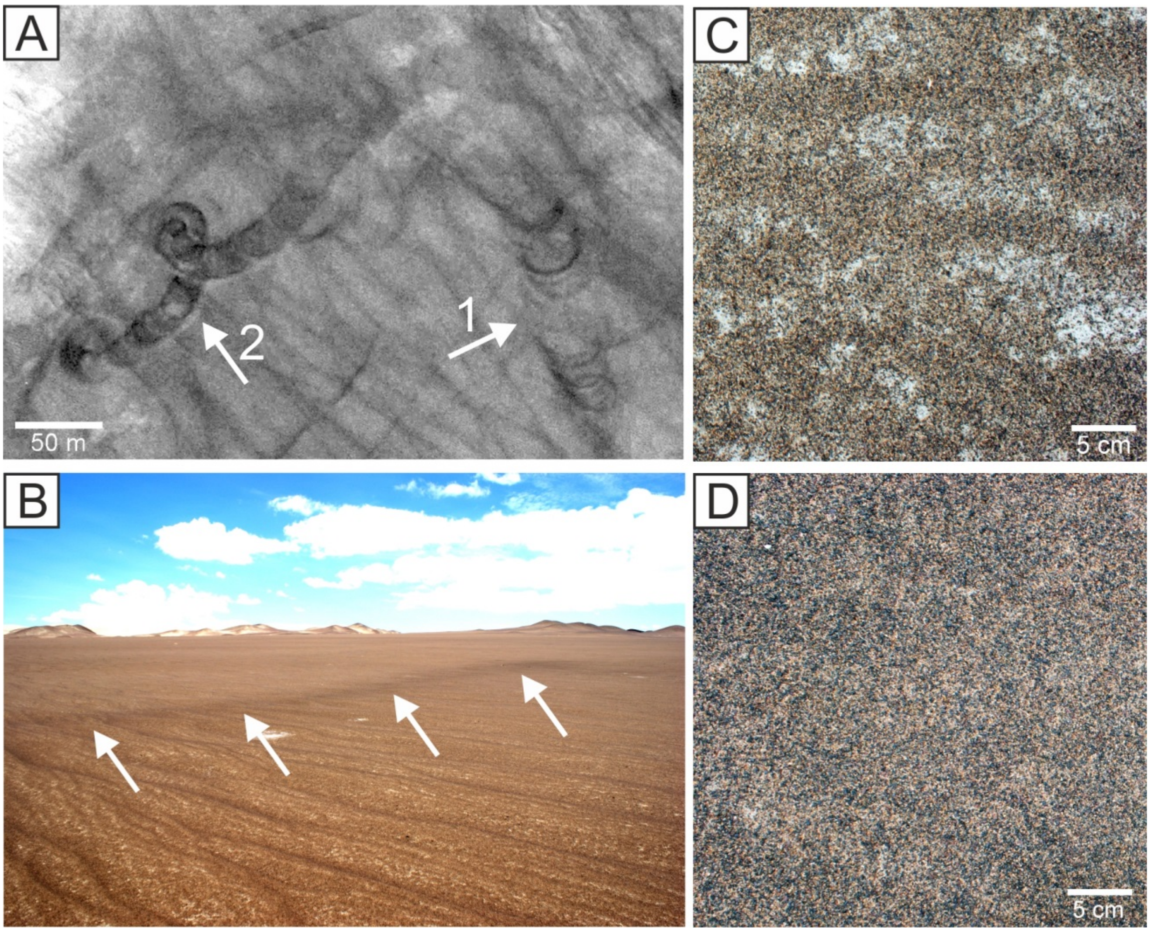

Figure 16. (A) Short-lived dark cycloidal DDT (arrow 1 and 2) in southern Peru at 14.2°S and 75.9°W (DigitalGlobe satellite image accessed through Google Earth). (B) Dark cycloidal DDT (white arrows) observed near the DDTs shown in A. (C) Top-view image of undisturbed ripple surface next to the DDT shown in B. (D) Top view image of the dark cycloidal DDT area shown in B. For further information see also Reiss et al. (2013).

Large-eddy simulations (LES) have revealed critical details of large-scale vertical convective vortices, including how interactions with the surface can lead to their considerable intensification (Lewellen et al. 2000; Lewellen and Lewellen 2007a; Lewellen and Lewellen 2007b), how massive loadings of debris can reorganize the momentum distribution and damage potential of a vortex (Lewellen et al. 2008), and how debris transport can leave behind visible deposits of debris, or surface marks (Michaels 2006; Lewellen and Zimmerman 2008). Most of these simulations have focused on the physics of tornadoes and their debris clouds, but a simple dimensionless scaling (Lewellen et al. 2008, Zimmerman and Lewellen 2010) allows the results to be scaled to terrestrial dust devils, though the latter are typically smaller and not as intense as tornadoes. This approach has allowed existing simulations of tornado tracks to be repurposed for studying how surface marks are generated by dust devils in the field (Reiss et al. 2013).

The dimensionless scaling between tornadoes and dust devils is enabled by several similar physical characteristics. Both classes of vortex are fed by a wide but shallow inflow layer that is relatively low in angular momentum compared to the embedding flow aloft. They also exhibit a corner flow region – where the near-surface flow intensifies while also turning rapidly upward – and a swirling, rising annular core aloft (Lewellen et al. 2000). Tornadoes and dust devils can accumulate large debris clouds that leave contrasting patterns of deposition on the ground (Lewellen et al. 2008; Zimmermann and Lewellen 2010; Reiss et al. 2013). A dimensionless parameterization applicable to tornadoes and dust devils has been discussed at length in (Lewellen et al. 2000; Lewellen et al. 2008; Zimmermann and Lewellen 2010; Reiss et al. 2013). Given a radius R_c and peak swirl velocity V_c in the upper core, a background angular momentum level Γ_∞ in which the vortex is embedded, a ground-relative translation speed U_t, the depleted flux of angular momentum Υ flowing into the corner from the surface layer, a surface roughness length z_0, a debris particle's terminal velocity w_t, and gravitational acceleration g, at least four dimensionless parameters can be formed:

1. Corner flow swirl ratio, $S_c = R_c \Gamma_\infty^2 / \Upsilon$, which determines whether the vortex is dominated by swirling flow or radial/vertical flow-through.
2. Translation ratio, $A_t = U_t / V_c$, defining the surface-relative translation speed as a fraction of the characteristic swirl velocity.
3. Acceleration ratio, $A_a = V_c^2 / g R_c$, scaling the characteristic centripetal acceleration to planetary gravity.
4. Debris type, $A_v = V_c / w_t$, which is a measure of how effectively debris can be entrained and lofted.

Simulations have revealed that leading aspects of the vortex are largely encoded within (1-4) (Lewellen et al. 2000; Lewellen and Lewellen 2007a; Lewellen and Lewellen 2007b; Reiss et al. 2013).

The particles comprising surface marks at the site of the Peruvian dust devil study of Reiss et al. (2013) were nearly monodisperse, with a size of 0.5 – 2 mm and mass density 2000 kg m^{-3}, making a direct comparison with large-eddy simulations (with a similarly monodisperse debris population) possible. To derive approximate dimensionless parameters associated with the dust devils observed in Reiss et al. (2013), and thus select the closest possible tornado simulation for comparison, the debris terminal speed, translation speed, core radius aloft, peak swirl velocity aloft, and near-surface depleted angular momentum flux must be estimated. Under terrestrial gravity, the terminal speed for a spherical grain in the size and density range of Reiss et al. (2013) is w_t=3.2-9.2 m s^{-1}. The observed dust devil tracks give an approximate width of the vortex (although in some simulated cases, debris can be thrown a considerable distance inward), setting R_c~25 m. Meteorological measurements of the Peruvian dust devils are not available, but a core velocity aloft V_c=25 m s^{-1} and translation speed U_t~4 m s^{-1} are tentatively assumed based on dust devil climatology (Balme and Greeley 2006). Together with g=9.81 m s^{-1}, these parameters set the ratios A_t=0.15, A_a=2.1-2.5 and A_v=2.7-2.8. It is impossible to estimate the near-surface flow properties required to derive S_c for the dust devils in Reiss et al. (2013); however, with set ranges for the other three dimensionless ratios, an attempt has been made to select the "best" swirl ratio that reproduces major characteristics of the surface tracks observed in the field.

Figure 17 shows a surface track from a large eddy tornado simulation with A_t=0.15, A_a=2.2, A_v=4.3, and S_c=9.3. This best matches the qualitative appearance of the surface track in Figure 13A. Sand is removed from the margins of the simulated track, carried inward, and deposited in cycloidal marks, which are preferentially laid down to the back and right of the vortex (with respect to an observer on the ground looking along the direction of travel of the vortex). This is consistent with laboratory experiments on dust devil track formation (Greeley et al. 2004). In the simulation that produced Figure 17 (and many others, cf. Zimmerman and Lewellen 2010), bands of alternating debris concentration swirl inward from a wide area across the surface. In the corner flow, some debris is unable to follow the upward accelerating flow and slips back to the surface, where it is deposited in sharp cycloidal bands. The remainder is lofted and centrifuged outward into the tornado's debris cloud, or in the case of a dust devil, the sand skirt. In Figure 17, some of this debris falls back into the right margin of the track, where it forms diffuse bands of deposition. The left-right asymmetry in the far-field deposition is due to a rightward and forward tilt of the vortex induced by surface-relative translation (Lewellen and Zimmerman 2008). The simulated debris field is infinitely deep in the case of Figure 17; that is, removal is limited only by the negative feedback between debris removal and air momentum. In the Peruvian case study by Reiss et al. 2013, the effective debris field of millimeter-size grains is probably much more limited. However, the comparison between Figures 17 and 14A demonstrates that cycloidal mark formation is consistent with inward transport of sand from the margins of the track.

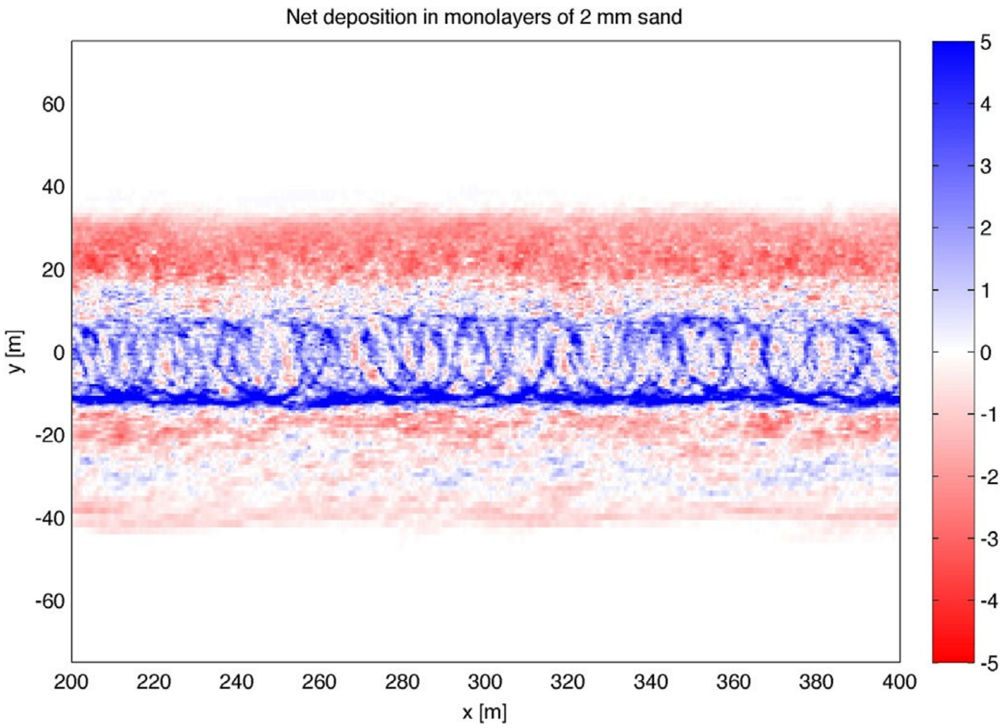

Figure 17: Simulated dust devil track (scaled from a LES tornado simulation). Positive and negative values correspond to net deposition and removal, respectively. Reproduced from Reiss et al. (2013).

Cycloidal dust devil tracks have been studied in the laboratory (Greeley et al. 2004) with the Arizona State University Vortex Generator (ASUVG). The ASUVG is a 2.5-m by 2.5-m moveable table assembly with an independently mounted motor and fan blade mounted in a cylindrical housing (see Figure 2 in Greeley et al. 2003). The table can translate both vertically and horizontally for simulating surface movement. The cylinder/fan-blade assembly can also translate vertically, which is used to control vortex parameters such as tangential wind speed and vortex diameter (Greeley et al. 2003). Previous experiments (Greeley et al.

2003) demonstrated that the ASUVG could replicate fundamental vortex morphology at lab scales at both Earth ambient and Mars analog conditions, including the characteristic ‘wobble’ of natural dust devils. The dust devil track experiments consisted of depositing a uniform, thin (400-800 µm thick) layer of ~125 to 200-µm silica sand on the test surface. In some experiments there was a 2-µm coating of red dust as well. As the ASUVG generated the vortex, the test surface was pushed beneath the rotating column of air, where the laboratory dust devil was allowed to interact with the sediment. Results showed a reorganization of the sand portions of the sediment, or the resulting ‘track’ left behind after passage of the vortex (Figure 18A). In many of the experiments, the resulting track was cycloidal in morphology and provided a sense of the movement direction of the vortex (Figure 18).

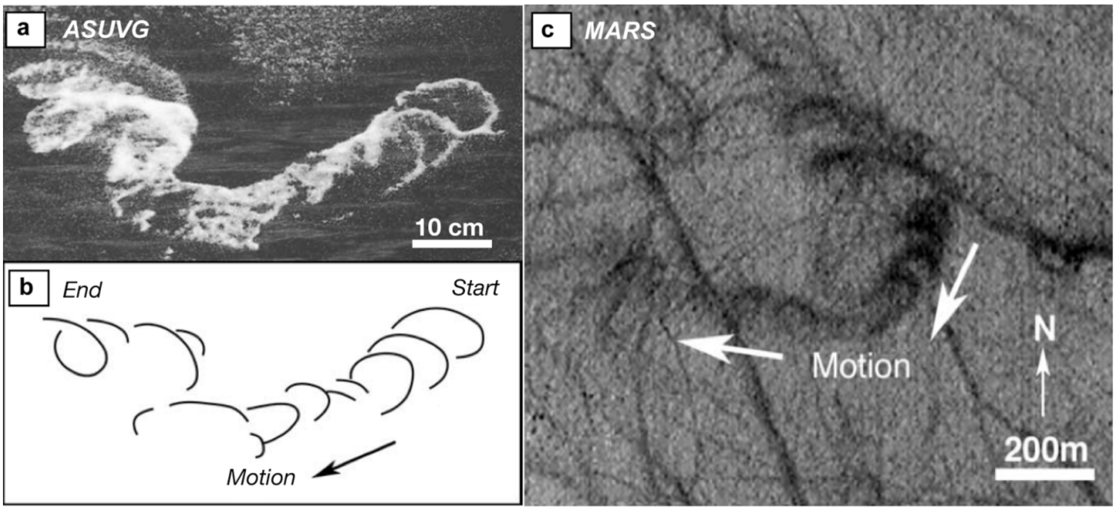

Figure 18. (After Greeley et al. 2004 and Neakrase 2009) a) Photo showing the experiment run with the ASUVG with 125-200 µm sand demonstrating the creation of a cycloidal track. b) Schematic cartoon of the ASUVG track. c) MOC-NA image (M10-03516) showing cycloidal tracks east of Hellas basin on Mars. **PERMISSION**

Analogous to the martian conditions, cycloidal tracks can be shown to be depositional features, primarily due to sand grains being reorganized by the dust devil. Larger particles that are initially lifted by the dust devil are too heavy to be lofted up into the column and are subsequently thrown out of the dust devil with angular momentum. The resulting pattern is a cycloidal track that opens in the direction of dust devil movement. This interpretation assumes that dust devils act both as an erosional and depositional agent, removing sand from the front of the dust devil and leaving the heavier particles in its wake.

Dark cycloidal DDTs are also observed on Mars (Figure 19), although they seem to be much rarer than dark continuous DDTs. Morphologically they resemble terrestrial dark cycloidal DDTs observed in southern Peru (Figures 14A, 15 A and 16A), indicating that they might be formed by the same mechanism process. Entrainment of sand on Mars is much more difficult than on Earth due to the low atmospheric pressure. The threshold shear velocity required to move sand grains with a diameter of ~200 µm in diameter by saltation under martian atmospheric conditions is ~1.5 m s^{-1} compared to 0.2 m s^{-1} for Earth (Iversen and White 1985; Kok et al. 2012). Wind speed measurements from martian landed spacecraft suggest that such shear velocities are rarely exceeded (e.g., Zurek et al. 1992; Holstein-Rathlou et al. 2010). However, there is much direct evidence that at least fine sand material is actively moved under present-day martian atmospheric conditions (e.g., Sullivan et al., 2008; Geissler et al. 2010; Silvestro et al., 2010; Bridges et al., 2011). Furthermore, dust devil tangential speeds can reach higher values than average martian wind speeds (e.g., Cantor et al. 2006; Choi and Dundas 2011), hence the redeposition of sand creating observed dark cycloidal DDTs on Mars seems plausible. However, direct evidence by in situ observations with rovers for this formation mechanism of dark cycloidal DDTs on Mars is lacking.

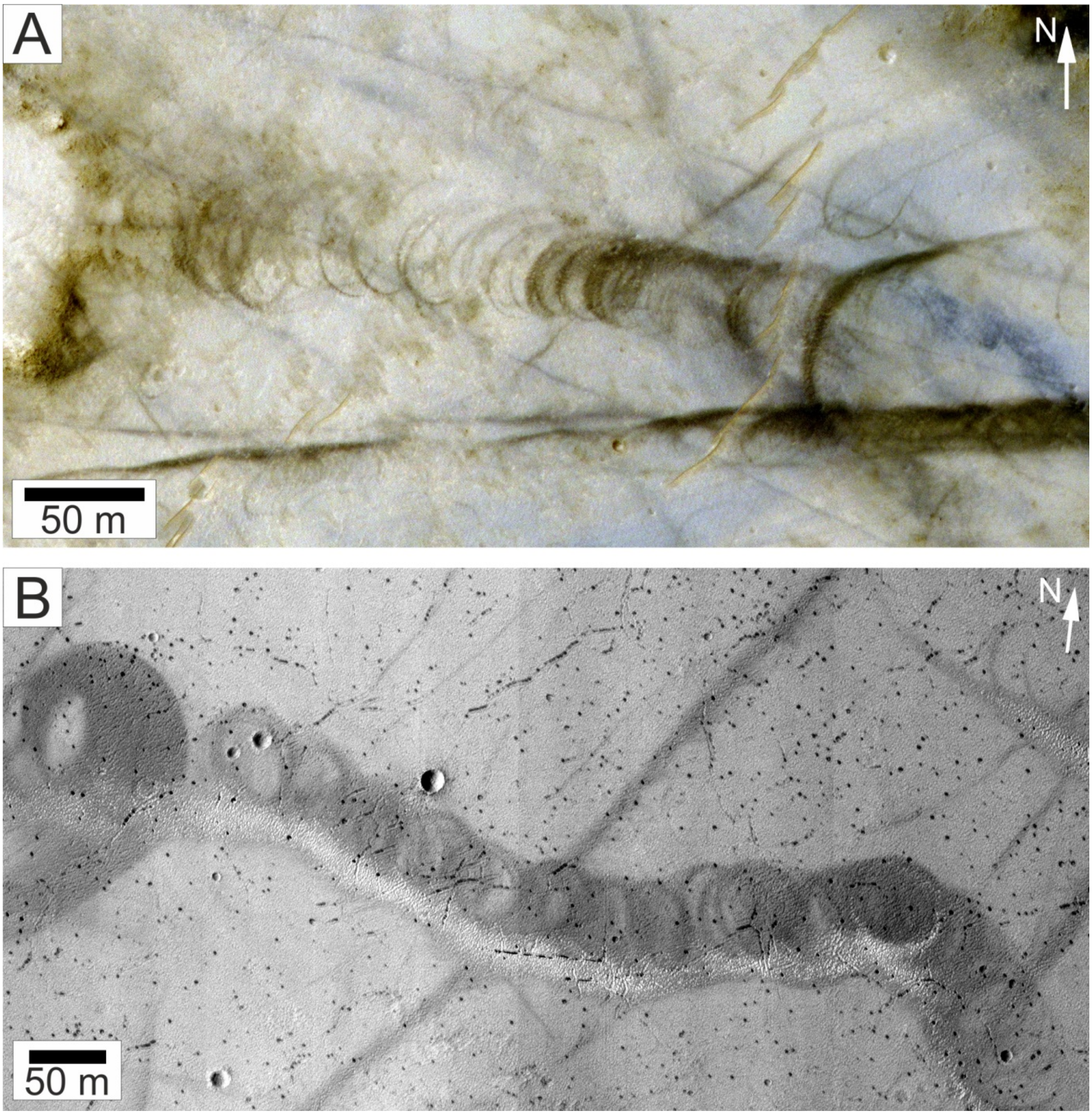

Figure 19. Dark cycloidal DDTs on Mars. (A) Dark cycloidal DDT in Schiaparelli crater at 5.2°S and 17.7°E (HiRISE image PSP_006477_1745). (B) Dark cycloidal DDT in Brazos crater at 5.6°S and 18.9°E (HiRISE image PSP_006477_1745). For comparison with terrestrial dark cycloidal DDTs, see tracks white arrows 1 and 2 in Figure 15A.

3. Spatial and temporal DDT distribution on Mars

Figure 20 shows a global map of Mars with the location and extent of DDT studies. Most studies did not discriminate between the different types of dark continuous, dark cycloidal and bright DDTs. In many cases only darker-toned DDTs were analyzed, because bright DDTs seem to be limited to dusty regions on Mars. Many studies also did not distinguish dark continuous from dark cycloidal DDTs, hence they are defined only as dark (dark toned or low albedo) DDTs.

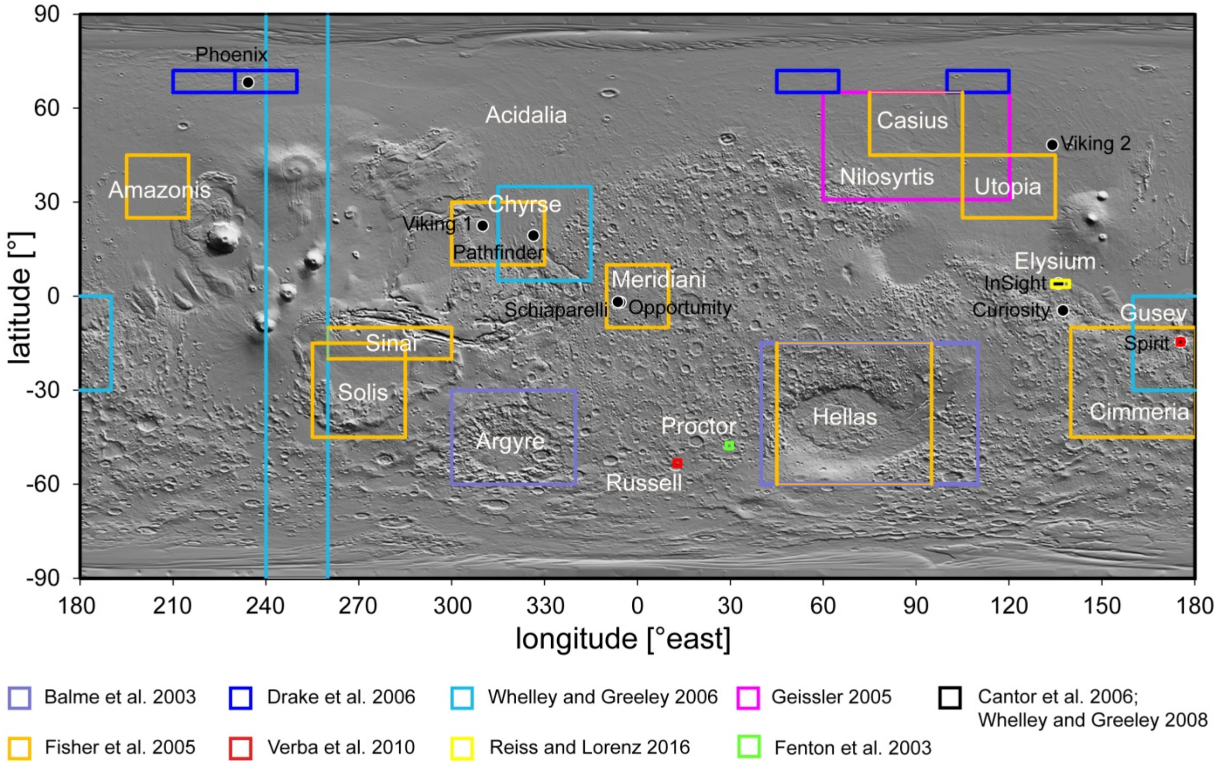

Figure 20. Location and extent of DDT study regions. Color extent and white text correspond to study regions given in the references. Black dots and black letters show the location and name of landed missions or future landing sites on Mars. Not included are the study regions of Ormö and Komatsu (2003) and Calef and Sharpton (2005) because they do not give specific statistics about DDTs.

3.1 Elevations

DDTs on Mars have been found to occur at all elevations, from the top of the tallest volcano (Olympus Mons) to the bottom of the deepest basin (Hellas Planitia) (Malin and Edgett 2001; Cantor et al. 2006). This is surprising because at high elevations the annual mean atmospheric pressure is only at around 1 mbar (avg. martian atmospheric pressure is around 7 mbar), but active dust devils and DDTs were observed in these low pressure environments (Cushing et al. 2005; Reiss et al. 2009), implying that dust devils can form even at very low ambient atmospheric pressures. Interestingly, Balme et al. (2003) found no correlation of DDT abundance with elevation in the study regions of Argyre and Hellas basin (elevations ranging from -6440 - +6130 m and -8208 - +4886 m, respectively), but this would be expected because increased atmospheric pressures at low elevations favor dust devil occurrence (Greeley et al. 2003). In addition, in a global study Whelley and Greeley (2008) did not find a correlation of DDTs with elevation. The reason for the independence of dust devil and DDT occurrence with elevation is unclear.

3.2 Seasonal occurrence

Dust devils form most frequently when insolation is around its seasonal maximum (e.g., Fisher et al. 2005; Cantor et al. 2006; Stanzel et al. 2008; Greeley et al. 2010; for a summary see also Fenton et al., this issue), hence DDT occurrence should exhibit a seasonal maximum during spring and summer. While most studies record the time when the image data containing DDTs was acquired, this does not provide the exact time of DDT formation (e.g., Balme et al. 2003). DDTs are likely formed prior to the image acquisition; hence the recorded seasons are probably actually later in the season. Balme et al. (2003) observed an increase of DDTs in the Argyre and Hellas Planitiae during early spring, followed by a more distinctive increase in late spring and reaching its maximum during summer, whereas in fall and winter only a few DDTs formed because insolation is then near its seasonal minimum. The same trend in seasonal DDT occurrence was observed by Fisher et al. (2005) and Whelley and Greeley (2006; 2008) in the northern and southern hemisphere, although higher frequencies in fall were recorded.

Local-scale studies have used repeat coverage of the same region, recording newly formed DDTs (Verba et al. 2010; Reiss and Lorenz 2016). This method gives a more precise determination of seasonal DDT formation. Using MOC-NA images of the Proctor crater floor (47°S and 30°E), Fenton et al. (2003; 2005) observed DDT formation only from mid spring through late summer (L_S = 223-354°). Verba et al. (2010) found that the DDT activity in Gusev Crater (14.6°S and 175.4°E) was mostly confined to a period between L_S = 235° and 12° (mid spring to early fall) with an peak activity at L_S = 245° (mid spring). In Russel Crater (53.3°S and 12.9°E) the active dust devil season ranged from L_S = 172° to 40° (around the start of spring to early fall) with peak activity at L_S = 316° (mid summer) (Verba et al. 2010). The seasonal differences in DDT ocurrence between Gusev and Russell Crater are probably caused by the latitudinal difference in location, in which Russell Crater receives more insolation at perihelion during the southern summer, whereas DDT formation starts earlier in Gusev Crater due to its location within the tropical zone (Verba et al. 2010). At the proposed InSight landing site in Elysium Planitia (3.9°N and 136.7°E), the seasonally limited observations did not allow a conclusion about seasonal DDT activity, but the analysis points toward activity throughout the year with peak activities in northern spring and southern summer (Reiss and Lorenz 2016), both probably related to the equatorial location of this region.

3.3 Distribution

Based on a global MOC-NA image survey, Cantor et al. (2006) observed DDTs in the latitude range between 80°S and 80°N; hence, DDTs can occur globally except on the permanent polar caps. This hemispheric dichotomy was also detected by Whelley and Greeley (2006) latitudinal analysis (pole-to-pole survey). On a global scale, Whelley and Greeley (2008) mapped around 55,000 DDTs in 1238 MOC-NA images, which were selected with a seasonally stratified random sampling technique. They measured the percentage of the surface area covered by DDTs per image. Their results show a seasonal peak in the percentage of DDT cover near 60° in both hemispheres (Figure 21). In the northern hemisphere, the peak areal coverage is 10% between 40°N and 65°N during northern spring and summer, whereas in the southern hemisphere the peak coverage is 92% during southern spring and summer in a latitude band between 45°S and 75°S (Whelley and Greeley 2008). Whelley and Greeley (2006; 2008) attributed this to the asymmetric solar heating on Mars because of the planet's orbital eccentricity, where the southern hemisphere receives about 40% more solar insolation during the southern summer.

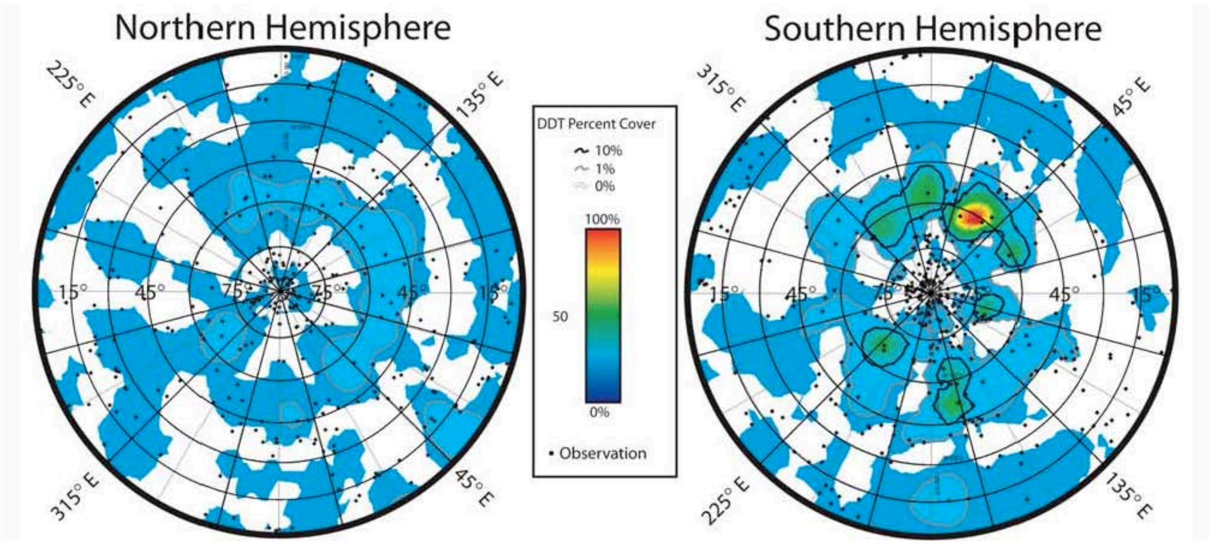

Figure 21. Interpolation maps showing the percentage of DDT image cover in spring and summer for the northern and southern hemispheres. Black dots indicate the location of analyzed MOC-NA images, isochrones and colors show the percentage of DDT coverage. From Whelley and Greeley (2008). **PERMISSION**

On a regional and local scale, the spatial DDT distribution can vary drastically. Drake et al. (2006) surveyed DDTs and wind streaks in four different regions, all located in the same latitudinal band between 65°N and 72°N. Although they did not distinguish between DDTs and wind streaks or give additional information about the seasonal coverage, the percentage of images containing these features varied from 3.5% – 20.9% (Drake et al. 2006). In another study, Fisher et al. (2005) analyzed active dust devils and DDTs in nine different regions located across Mars using MOC-NA imagery. They showed that all DDT detections were seasonally separated, although individual tracks were not counted. The maximum percentage of images containing DDTs in one season between the regions varied from 0.79% – 52.17% (Fisher et al. 2005). In some regions such as Casius, more than 50% of the images contained DDTs in two of four seasons, whereas in other regions such as Utopia, only 1% of the images contained DDTs in one season and 0% in the other three seasons (Fisher et al. 2005). The same strong variations of DDT occurrences can also be found within study regions. For example, Geissler (2005) analyzed MOC-NA images in the Nilosyrtis study area (60 - 120°E and 30 - 65°N) and observed a strong zonation of DDT occurrence confined to latitudes between 45°N and 65°N. DDT areal densities can vary even on a scale of 10s of kilometers: Fenton et al. (2003) found that dark continuous DDTs were plentiful in all but the northern area of Proctor crater floor, where none were visible.

3.4 Areal Density

The hemispheric asymmetry and strong regional spatial variations in DDT occurrence on Mars are also reinforced by statistically studies that normalize the number of DDTs by surface area, expressed as the number of DDTs per square kilometer. Whelley and Greeley (2006) mapped DDTs in MOC-NA images in a pole-to-pole survey and in some other regions in both hemispheres (Figure 20). They calculated average densities of 0.6 DDTs/km^2 for the southern and 0.06 DDTs/km^2 for the northern hemisphere. In addition, they measured regional differences with peak seasonal densities of about 0.02 DDTs/km^2 in Ares Vallis and about 0.1 DDTs/km^2 in Gusev Crater (Whelley and Greeley 2006). In the Hellas and Argyre basins, DDT densities showed a latitudinal zonation, often reaching 50 – 100 DDTs/km^2 in the southern areas of both study regions compared to values of less than 1 – 5 DDTs/km^2 in the northern areas (see also Figure 4 in Balme et al. 2003). The average density from one continuous year was 0.81 DDTs/km^2 for Argyre and 0.47 DDTs/km^2 for Hellas although densities in both study regions reached seasonal peaks of about 2.5 DDTs/km^2 (Balme et al. 2003).

On a local scale, repeat imaging of the same surface areas with high-resolution image data such as HiRISE (limited to interesting areas or landing sites) provides information of DDT formation rates expressed as DDTs/km²/sol (in which one sol is one martian day). Using this technique, Verba et al. (2010) mapped newly formed DDTs between image observations in Russell and Gusev Craters over the course of a martian year, calculating seasonal DDT formation rates. Formation rates ranged from 0.0011 to 0.103 DDTs/km²/sol in Gusev Crater and from 0.04 to 0.95 DDTs/km²/sol in Russell Crater (Verba et al. 2010). Reiss and Lorenz (2016) used the same technique to derive DDT formation rates at the proposed InSight landing site. They calculated formation rates from 0.002 to 0.08 DDTs/km²/sol (Reiss and Lorenz 2016). The much higher formation rates in Russell Crater relative to those in Gusev Crater and the InSight landing site shows large variability in DDT frequencies on a local scale.

As discussed above, local, regional, and global variations in DDT densities can partly be explained by their latitudinal location, which controls the receivable insolation, controlling dust devil generation, hence also DDT densities. However, the large regional variations in DDT distributions and densities are not so easily explained as DDT distributions and densities vary strongly between study regions within the same latitudinal band or within individual regions (Balme et al. 2003; Drake et al. 2006; Geissler et al. 2005). Furthermore, one study analyzed the frequency of active dust devils versus DDT abundance within several study regions, revealing a large discrepancy (Fisher et al. 2005). For example, in the Casius study region, no active dust devils were observed but many DDTs were, whereas in the Amazonis Planitia, many active dust devils were observed but only a few DDTs were detected (Fisher et al. 2005). The probable reason causing these large local, regional and global discrepancies in DDT densities and dust devil occurrences are discussed in the following section.

3.5 Thermophysical surface properties

Because DDT distributions and densities are not always consistent with dust devil activity, researchers suggested relatively early on that DDTs are not solely controlled by dust devil activity but by differences in surface materials, such as dust cover thickness or underlying substrate properties (Balme et al. 2003; Fisher et al. 2005; Whelley and Greeley 2006; 2008). Most DDTs on Mars are dark continuous tracks suggested to be formed by dust erosion, which exposes a substrate of relatively coarse-grained material (see section 2.1). If the dust layer is too thick, a passing dust devil may not be strong enough to expose the underlying substrate, hence no DDT would be formed. On the other hand, thin dust layers may enable even weak dust devils to expose the substrate, leading to areas with many DDTs. Another factor contributing to the formation of dark continuous DDTs is that on Earth the distribution of DDTs seems to be controlled by the particle-size difference between the substrate material to the lofted material (Reiss et al. 2010). The substrate material needs to be sufficiently large enough relative to the lofted grains to create albedo differences by photometric changes (see section 2.1). For example, terrestrial studies have shown that dark continuous DDTs occur only in areas where the substrate consists of coarse to very coarse sands, and no DDTs are observed in areas consisting of fine sand grains, implying that when particle sizes of the substrate materials are too small, the photometric effects are not large enough to create visible albedo contrasts between the track and the undisturbed area (Reiss et al. 2010; 2012).

The distribution of identified DDTs on Mars can be compared to derived global thermophysical data sets, such as Thermal Emission Spectrometer (TES) albedo maps (Christensen et al. 2001), thermal inertia maps (Mellon et al. 2002; Putzig et al. 2005), and dust cover index (DCI) maps (Ruff and Christensen 2002). For example, Balme et al. (2003) found that the distribution of DDTs in the Argyre and Hellas study were correlated with surfaces indicative of a thin dust layer, suggesting that dust availability controls the abundance of DDTs. Whelley and Greeley (2006; 2008) found that DDTs correlate with high thermal inertia (interpreted to be rocky) in the southern hemisphere, but with low thermal inertia (interpreted to be dusty) in the northern hemisphere. This suggests that a high thermal inertia surface with a thin dust cover is not a prerequisite for DDT formation and a low thermal inertia surface with a relatively thick dust cover does not preclude DDT formation (Whelley and Greeley 2008). Reiss (2014) surveyed DDTs in MOC-NA images with a resolution of <3 m/pxl in the equatorial region (latitude range from 30°S to 30°N) and compared the geographic location of images containing dark or bright DDTs with these areas' themophysical surface properties (Figure 22). Results showed that bright DDTs occur in areas of high albedo (~0.28), low thermal inertia (~75 J m^{-2} $s^{-1/2}$ K^{-1}), and high dust cover (DCI~0.94), whereas dark DDTs occur in areas of moderate albedo (~0.2), moderate thermal inertia (~250 J m^{-2} $s^{-1/2}$ K^{-1}), and moderate dust cover (DCI~0.96), indicating that bright DDTs occur in regions with a relatively thick dust cover and dark DDTs in regions with a relatively thin dust cover (Reiss 2014).

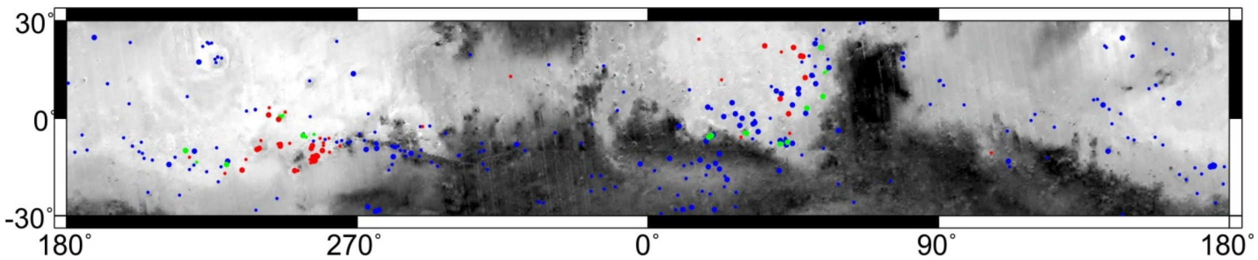

Figure 22. Distribution of dark and bright DDTs from a MOC-NA survey (Reiss 2014). Blue = dark DDT; Red = bright DDT; Green = dark and bright. Small circles = few DDTs; Large circles = many DDTs. Background: TES Albedo (Christensen et al. 2001).

4. DDTs as proxies

4.1 Dust devil activity

Inferring dust devil activity from DDT frequencies is difficult because DDT formation is, amongst others factors, controlled by surface properties (see section 3.5). This is probably one of the main reasons why there are large regional variations in DDT densities (see also section 3.4). Another reason why it is difficult to infer dust devil activity from DDTs is that only intense dust devils (e.g., high tangential wind speed, large pressure deficit or high vertical wind speed within the core) are able to create tracks if the dust layer is several microns thick, meaning that using DDTs as a proxy for DD frequency underestimates the actual number of dust devils. Furthermore, the horizontal ground speeds of dust devils are controlled by ambient wind speeds (e.g., Balme et al. 2012; Reiss et al. 2014a), which define how long a dust devil crosses a specific point at the surface; hence, local or regional variations in wind speeds directly influences the formation of DDTs. Direct observations of active dust devils on Mars show that on a global scale, only ~14 % leave tracks (Cantor et al. 2006). However, on a regional or local scale, large variations can be expected. Verba et al. (2010) compared measured DDT formation rates with directly observed active dust devils by the MER Spirit (Greeley et al., 2006b; 2010) in Gusev Crater, implying that only every 100th to 500th dust devil is able to leave a track. Therefore, deducing dust devil activity from DDTs is problematic. However, global calculations using DDT frequencies as a proxy for dust devil activity and derived calculations of the contribution to dust entrainment on Mars (Whelley and Greeley 2006; 2008) may give first-order estimates on a global scale (see also Klose et al., this issue).

4.2 Dust devil durations

The duration of dust devils on Mars can be calculated by measuring their translational ground speeds (see also Fenton et al. 2016, this issue) and their adjacent DDT lengths. Such derived dust devil durations are only minimum values, however, because the observed dust devils used as end points are still active. Other uncertainties surround the DDT starting points, because the corresponding dust devils might have been active before they started forming tracks. Nevertheless, these calculation methods are powerful tools for determining dust devil durations. They were used by Stanzel et al. (2008), who observed four dust devils in HRSC images and measured their translational ground speeds and adjacent DDT lengths, thereby calculating minimum dust devil durations in the range of 3.7–32.5 minutes. In addition, they used eight additional DDT length measurements in the vicinity of the four dust devils to derive a mean minimum durations of 13 minutes (Stanzel et al. 2008). In a later study, Reiss et al. (2011b) examined one large dust devil (diameter of ~820 m) on HRSC images. After measuring the translational ground speed and an adjacent DDT length, they calculated the dust devil minimum duration to be 74 minutes. Dust devil durations can be additionally estimated from measured DDT lengths and widths using a dust devil longevity-diameter relationship (Lorenz 2013) in combination with assumed translational ground speeds (Lorenz and Jackson 2016). These studies show that, compared with direct duration measurements of smaller dust devils in Gusev crater by Greeley et al (2006; 2010), larger dust devils are active longer than smaller ones (Reiss et al., 2011b, see also Fenton et al. 2016). For a summary of terrestrial and martian dust devil durations, we refer here to Lorenz et al. (2013). Additional information about the influence of dust devil longevity and DDT lengths can be found in Lorenz and Jackson (2016).

4.3 Ambient Wind Directions

The orientation of DDTs can be used to infer wind directions because dust devils move approximately parallel to the ambient wind field (e.g., Wegener, 1914; Flower, 1936; Crozier, 1970; Balme et al., 2011; Reiss et al., 2014). Precise wind directions without the need of climate models can be inferred directly from imaged active dust devils leaving tracks in their wakes or from the morphology of cycloidal DDTs (Greeley et al. 2004; see also section 2.3). However, most DDTs are dark continuous tracks in which the wind direction is ambiguous, e.g., west-east oriented DDTs would indicate winds from the west or east. On Earth, DDT orientations in the Ténéré Desert were compared with regional winds inferred from wind streaks, but no correlation was found (Rossi and Marinangeli, 2004). However, wind directions during the formation of the DDTs from (for example) meteorological stations were unknown and might have been consistent with observed DDT orientations. On Mars, Fenton et al. (2005) used the PSU/NCAR 5th generation mesoscale model (MM5) to show that dust devil tracks that form on the floor of Proctor crater during spring and summer are oriented to light mid-latitude westerly winds that blow during the early afternoon in these seasons. Drake et al. (2006) provided an estimate of wind directions from the orientation of DDTs for the Phoenix landing site candidates. Later, DDT orientations in Mars's Gusev and Russell craters were measured and compared with wind direction predictions from the NASA Ames general circulation model (GCM); for active dust devil seasons, estimates made using the DDT orientations offered good agreement with the predicted wind directions (Verba et al., 2010). More recently, DDT orientations at the InSight landing site region were compared with the Mars Climate Database (MCD) wind direction predictions (Reiss and Lorenz, 2016). The resulting seasonal comparison between the DDT alignment and the MCD-predicted wind directions showed that dust devils moved from SE to NW until early northern autumn, and then they reverse directions and move from NW to SE at around L_S = 200°, consistent with the seasonal reversal in direction of the Hadley circulation (Reiss and Lorenz 2016). In general, seasonal ambient wind fields can be directly inferred from DDT orientations in combination with wind direction predictions from atmospheric models. Such direct deductions of wind directions from DDT measurements reflect the real ambient wind fields during the DDT formation times and are more accurate than climate model predictions, especially during times when regional weather fronts are active (e.g., Reiss et al. 2014), which are not resolved in climate models.

4.4 Surface Wind Conditions

The shape of DDTs can probably be used to infer surface wind conditions. DDTs exhibit large variations in plan-view of linear, curvilinear, curved, meandering or looping track patterns (see section 2.1). Terrestrial field measurements showed that dust devils have a greater variability in the ground track direction at lower ambient wind speeds (Balme et al. 2012). Lorenz (2016) showed that dust devil migration directions are consistent with a 'random' component of motion associated with convection vector-added to the ambient wind. Hence, at lower ambient wind speeds and /or high random component curved or looping track patterns should be formed, whereas at larger ambient wind speeds and/or small random component linear DDT morphologies should be expected. This relationship and its effect on in-situ measurements (pressure drop) are discussed in detail in Lorenz (2013). One parameter for the classification of DDT shapes is the sinuosity (ratio between the DDT length measured (a) along the total path length and (b) as a straight line from the start and end point). Verba et al. (2010) measured a DDT mean sinuosity of ~1.3 and ~1.08 in Russell and Gusev Crater, respectively, and Reiss and Lorenz (2016) measured a mean sinuosity of ~1.03 at the InSight landing site region in Elysium Planitia. This would suggest higher ambient wind speeds in Elysium Planum and Gusev Crater than in Russell Crater. Such a relationship between the sinuosity of DDTs and ambient wind speeds could ideally be tested in future LES simulations (see Spiga et al. 2016, this issue).

4.5 Solar panel clearing predictions

The power supply of many landers or rovers on Mars is provided by solar arrays. Atmospheric dust deposition on the solar panels causes a decline in electrical power output with time (e.g., Landis and Jenkins, 2000; Crisp et al., 2003). Without solar panel clearing events by wind gusts or dust devils, lander or rover science operations can be limited as it has been the case for the Spirit (MER – A) rover at Gusev crater (e.g., Greeley et al., 2010). Lorenz and Reiss (2015) showed that intense dust devils were primarily responsible for recurrent solar panel clearing events (recurrence interval of 100 – 700 sols) at Gusev crater. DDTs can serve as a proxy for solar panel clearing recurrence interval estimates, because the formation of dark continuous DDTs by the removal of a thin layer of dust is in principle the same process a clearing of dust from solar panels. Reiss and Lorenz (2016) mapped newly formed DDTs in repeat HiRISE image observations covering the same surface area at the InSight landing site region. Calculated seasonal DDT formation rates (in DDT km^{-2} sol^{-1}) and DDT area formation rates (in DDT km^{-2} km^{-2}) give estimates how often DDTs are formed and how often a specific point on the surface is crossed by an intense dust devil (able to leave a DDT), respectively (Reiss and Lorenz, 2016). Measured DDT formation rates were used to find a scaling factor to the calculated seasonal dust devil activity (DDA) index (Renno et al., 1998), which is defined as the flux of energy available to drive dust devils estimate seasonal dust devil activity, and then integrated over the year to estimate a mean annual DDT formation rate for the InSight landing site region (Reiss and Lorenz, 2016). As a result, a maximum solar panel clearing recurrence interval of ~11 Mars years was estimated (Reiss and Lorenz, 2016). Applying the same technique for Gusev Crater using measured DDTs of Verba et al. (2010) gives average solar panel clearing recurrence interval of ~160 sols (Reiss and Lorenz 2016). This is in relatively good agreement with solar panel dust clearing events (Vaughan et al., 2010) and with the calculated recurrence interval of 100–700 sols for intense dust devils (pressure drop > 6 Pa) (Lorenz and Reiss 2015) at the MER Spirit rover in Gusev crater, indicating that DDTs can be used effectively as a proxy to predict the rate of solar panel clearing events. However, such estimated solar panel clearing recurrence intervals by dust devils from DDTs should be seen as an upper limit, because less intense dust devils not able to leave tracks likely contribute in clearing dust on solar panels (Reiss and Lorenz 2016).

5. Impacts on Mars Climate

It has long been recognized that minute amounts of dust can significantly alter the spectral and photometric properties of the martian surface; for example, the reflectance at 0.56 μm of a typical dark region on Mars will increase by 35% after dust deposition of only $9x10^{-5}$ g/cm^2 (Wells et al. 1984). As a result, fallout from dust storms, particularly that from global-scale events, can brighten the surface, often increasing the albedo of large regions by several percent or more (e.g., Christensen 1988; Smith 2004; Geissler, 2005; Szwast et al 2006). Eventually, and often episodically, these dust deposits are swept away during local dust storms, along storm fronts, or by regional winds enhanced by topography or albedo contrasts (Geissler 2005; Szwast et al. 2006). These changes in the albedo impact more than just the surface, however. For example, surface brightening caused by fallout from the 2001 global-scale dust event decreased daytime surface and atmospheric temperatures that lasted long after the storm itself abated (Smith 2004). Atmospheric modeling indicates that the observed albedo changes on Mars influence annual mean near-surface air temperatures and wind stresses, which in turn affect dust lifting (Fenton et al. 2007). As a result, the albedo changes caused by dust erosion and deposition may be regarded as a dynamic climatological variable that is critical to understanding the martian climate system (Szwast et al. 2006).

Within dark DDTs, the surface albedo can be as much as ~3% lower than that adjacent to the tracks (Statella et al., 2015, see also section 2.1). Geissler (2005) observed dark DDTs in some of the regions where the surface albedo had decreased, and attributed part of the observed regional darkening to their occurrence. However, Szwast et al. (2006) argued that dust devils and other small-scale lifting processes are not capable of significantly changing global patterns of dust cover (a recent study by Geissler et al. (2016) concedes this point). In the areas debated by Geissler (2005) and Szwast et al. (2006), the seasonal (local spring and summer) peak percentage covered by dust devil tracks is ~10% (Whelley and Greeley 2008), suggesting that dust devils are less effective at removing dust than other processes. However, the regions on Mars most densely covered by seasonal dust devil tracks are in the southern mid- to high-latitudes, where the seasonal peak coverage percentages reach up to 92% (Whelley and Greeley 2008). It is more plausible that dust devils significantly contribute to surface erosion and albedo darkening in the southern hemisphere, although their impact has not yet been investigated. In addition, DDTs may more significantly alter surface albedos in specific, smaller-scale regions, such as on dark dunes (Bennett et al., in review).

Haberle et al. (2006) ran simulations from a general circulation model (GCM) based on the NASA/Ames GCM (Kahre et al. 2006), both for present-day Mars and under orbital conditions of the past, when Mars' longitude of perihelion was opposite that of today (i.e., perihelion occurred near northern summer solstice rather than the current position just prior to southern summer solstice at L_s = 251°). Using a parameterization of dust lifting by dust devils based on the thermodynamic model of Rennó et al. (1998), Haberle et al. (2006) modeled the seasonal pattern of dust entrainment for the different martian orbital states. The present-day case predicts a significant amount of dust lifting during the southern summer; the other two cases predict a lower but more seasonally balanced rate of dust lifting. It is likely that as

Mars' orbit forces climatic shifts to occur, the rate of dust devil (and dust devil track) production will vary in frequency and with location on the planet. If dust devil tracks do indeed contribute significantly to changes in surface albedo in some regions, then they are one of many factors influencing climate change on Mars.

6. Automatic detection of DDTs on Mars

As more successful missions are launched to study Mars, the amount of remotely sensed data we have for Mars also rises. Previous missions have produced thousands of orbital images depicting the martian surface, which requires automated analysis approaches in order to quickly and accurately extract relevant information from the data.

Once such automated method for detecting martian DDTs in digital images was presented and evaluated by Statella et al. (2012). This method, mainly based on Mathematical Morphology, is based on the following steps: filtering, track candidate selection, track candidate enhancement and track detection. The method was tested on MOC-NA and HiRISE images. The first step is filtering using the morphological surface area opening and surface area closing operators in order to attenuate the high reflectance of boulders, ripples and the dark spots caused by their shadows. In Figure 23B and C the bright faces of boulders and their shadows have been suppressed from the original (cropped) HiRISE image (Figure 23A).

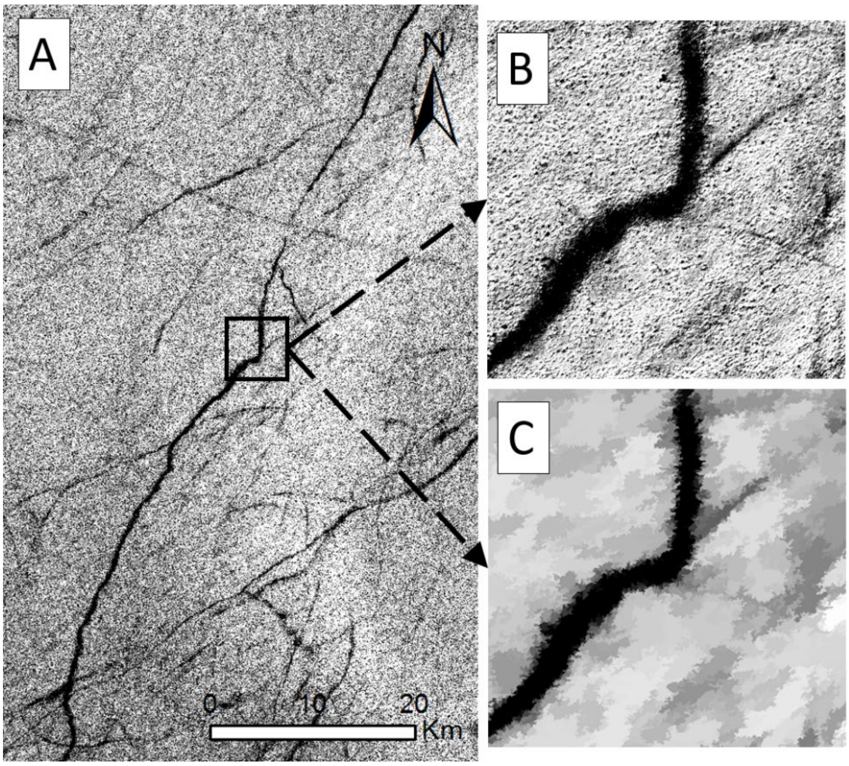

Figure 23. Filtering step: (A) original HiRISE image ESP_013557_1245; (B) detail of (A) and (C) the result after filtering. The rectangle annotated in (A) indicates the region selected for the details shown in (B, C).

In the next step, a morphological path closing (Hendriks, 2010) with a specified length and oriented in the four directions (0°, 45°, 90° and 135°) is applied for the selection of all possible dark paths. This is performed in an indirect way, since all the desired long dark structures are suppressed (Figure 24A). The considered paths are not strictly straight lines, as they are allowed to deflect inside a 90° aperture cone centered in each of the four adopted directions of search. The maximum lengths of the paths are defined by the dimensions of each image and calculated as $\sqrt{m^2 + n^2} \times 2$, where m and n are the number of columns and rows of the image, respectively.

In the third step, the dark paths are then recovered and enhanced by a morphological top-hat (difference between the closed image, in which the tracks were removed by the path closing, and the original image) transformation (Figure 24B). This grey level output must go through a thresholding to become a binary image that shows only the dust devil tracks. For that purpose, Statella et al. (2012) applied an Otsu's algorithm (Otsu, 1979) constrained to look for a threshold in the interval $[k_{mean}, k_{\max}]$ of the histogram. Such intervals were defined based on a preliminary analysis of the binarization performance; the binarization by the constrained Otsu's algorithm is shown in Figure 24C. The method was applied to 90 MOC NA and 110 HiRISE images, from which 2 original images and detection results are shown in Figure 25.

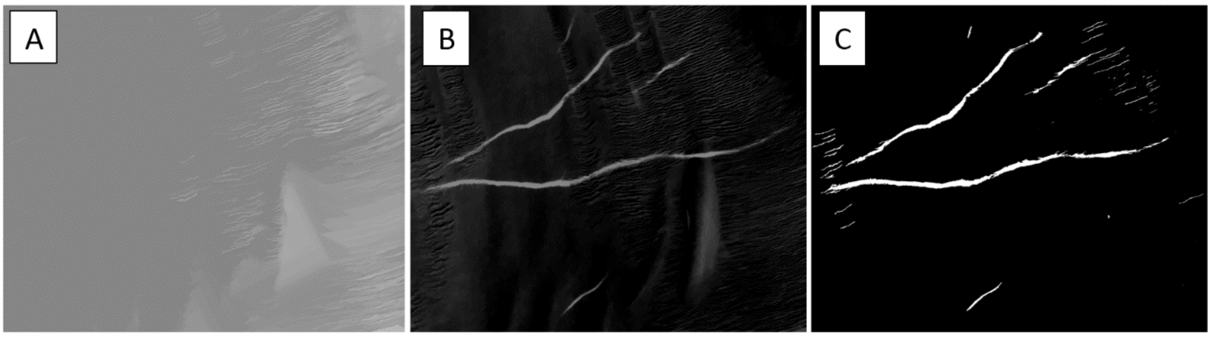

Figure 24. (After Statella et al. 2012) Selection of DDT candidate, enhancement and binarization: (A) Path closing transformation suppresses the candidates; (B) Top-hat by closing recovers and enhances the candidates; (C) A constrained Otsu's method is applied for the segmentation of the tracks.

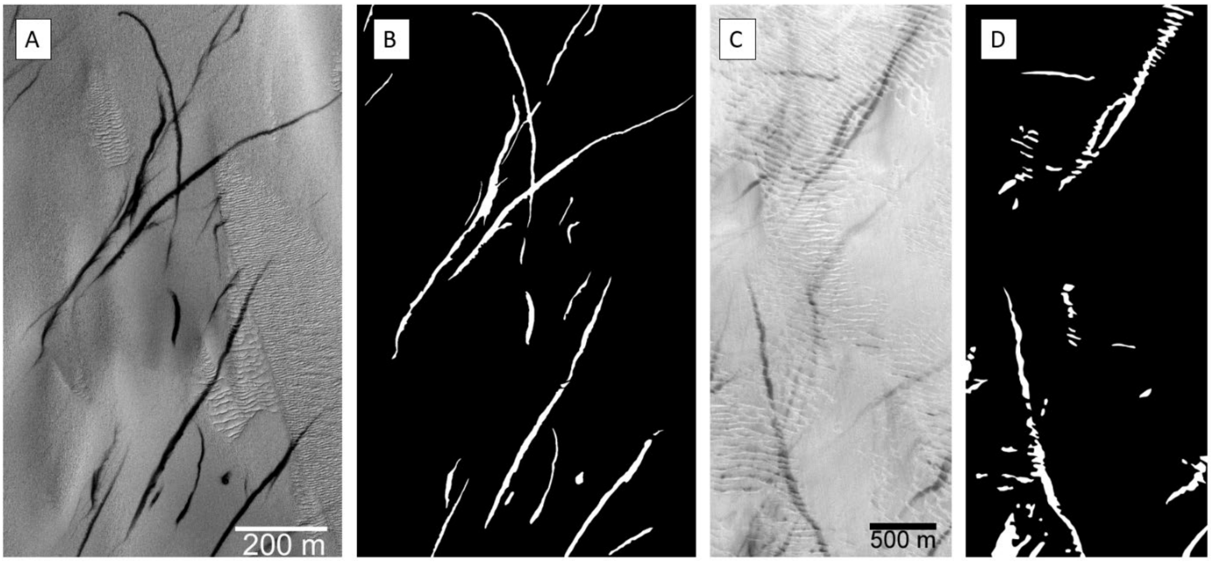

Figure 25. (A and C) Original HiRISE (PSP_006163_1345) and MOC (M10-01206) images. (B and D) Corresponding images that have been processed by the proposed method. Images B and D are binary and show pixel tracks in white and background in black.

The results were analyzed according to the procedure proposed by Bandeira et al. (2011). For each of the 200 processed images, a ground truth image was constructed manually in order to estimate the global accuracy of the method using pixel based comparison (Statella et al. 2012). The mean global accuracy after processing the 200 images was 92.02% ± 4.87%. The lowest accuracy was 69.15% and the highest was 99.34%. The accuracy was not affected by the variation in spatial resolution of the images and is not sensitive to variations in latitude and solar longitude. The results show that the measure of ~92% ± 5% for the detection process allows the features to be estimated accurately. Therefore, the method can be a very useful tool for intensively mapping dust devil tracks.

Then, the availability of black and white images with the detected tracks allows extracting their characteristics in an exhaustive way. Automated approaches have been developed to obtain those features in an extensive way using information from of the whole detected tracks including average widths, lengths and orientations. These methods permit to better describe the dust devil tracks, namely, by inferring their direction of movement (Statella et al., 2014), estimating the albedo contrast with their neighborhoods (Statella et al., 2015) or computing the distribution of widths (Statella et al., 2016).

7. Summary and Future Directions

DDTs exhibit a linear to curvilinear, curved, meandering or looping but not entirely straight morphology in plan-view, which makes it relatively easy to differentiate them from aeolian wind gust streaks. On both Earth and Mars, their sizes typically reflect the width and duration of dust devils (see also Fenton et al. 2016, this issue), and they have widths that range from one to hundreds of meters and lengths of up to several kilometers. They can be classified into three different types based on their morphology and albedo: (a) dark continuous, (b) dark cycloidal, and (c) bright DDTs. All three types can be found on both planets, although terrestrial DDTs are rarely observed.

The most common type of DDT on Mars is dark continuous DDTs, which have been observed on both planets in satellite imagery and analyzed in situ by MER Spirit on and on Earth. Both studies revealed that dust erosion by dust devils exposes coarser grained substrate consisting of coarse sand particles (0.5 < particle diameter < 2mm), which changes the photometric properties of the surface and leads to low albedo track areas in contrast to the undisturbed surroundings. The formation mechanism of dark continuous DDTs is only based on one in situ study on each planet, so we can not exclude alternative effects, such as compositional differences between the eroded dust layer and the exposed substrate or additional effects such as redistribution. Further in situ investigations of dark continuous DDTs on both planets would help verify the proposed formation mechanism. Dust deflation calculations as well as numerical simulations indicate that removing an equivalent dust layer thickness of around 1 µm would be sufficient to cause albedo differences that lead to visible tracks on Mars. On Earth, measured values are similar, requiring the removal of an equivalent dust layer having a thickness of 1 – 2 µm. Future measurements that can quantify the dust deflation thickness within dark continuous DDTs would be very helpful for improving estimates about how much dust devils contribute to dust entrainment in the atmosphere, especially on Mars (see also Klose et al. 2016, this issue). DDTs are visible due to the lower albedo track relative to the adjacent terrain. Measurements of albedo differences between the track area and the undisturbed surrounding terrain have rarely been conducted. Mean albedo contrasts are in the range of ~ 2.5 % wavelength range 550 – 850 nm) on Mars and around 0.5% (wavelength range 300 to 1100 nm) on Earth. Further albedo contrast measurements would help quantify larger-scale albedo changes that influence the recent climate on Mars. The lifetime of dark continuous DDTs is sub-annual on both planets and depends on atmospheric dust deposition rates, as deposited dust obscures tracks. This track obscuration can happen relatively quickly after dust storm events because of increased atmospheric opacity and dust settling rates.

The second type of DDT, dark cycloidal DDTs, can be observed on Mars and Earth in satellite imagery. In plan-view morphology, they resemble tornado tracks on Earth, and terrestrial in situ studies revealed that they formed when sand-sized grains that has eroded from the outer vortex area is redeposited in annular patterns in the central vortex region. Terrestrial dark cycloidal DDTs can be either short- or long-lived; they exhibit sub-annual lifetimes on aeolian active surfaces, but they can be visible for several years on aeolian inactive surfaces. On Mars, neither in situ studies nor specific studies have been conducted to date. The proposed formation mechanism for these DDTs on Mars (re-deposition of sand) has only been suggested from terrestrial analog, laboratory, and modelling studies. Thus, to confirm the proposed formation mechanism, in situ studies on Mars carried out by future rover missions would be necessary. However, this would require that dark cycloidal DDTs occur close to the rover landing site, which is unlikely. But, in the near future, specific studies on martian dark cycloidal DDTs, based on satellite imagery and combined with numerical modelling seem to be most promising method to verify the proposed formation mechanism and to determine their lifetimes.

The third type of DDT, bright DDTs, are brighter than their surroundings and occur on both planets. However, in situ studies have so far only been conducted on Earth, and they indicate that surficial aggregates of fine particles are destroyed by passing dust devils, which causes changes in the photometric properties inside the track area (i.e., smooth surfaces inside the track versus rough surface texture of the undisturbed surroundings). Based on this terrestrial analog, the same formation mechanism might also be valid for the formation of the bright martian DDTs, because in situ studies provided evidence of surficial dust aggregates that can easily be lofted and destroyed by passing dust devils. Furthermore, the distribution of bright DDTs on Mars seems to be predominantly in regions with a relatively thick dust cover. However, the lack of in situ studies on Mars leaves the formation mechanism of the martian bright DDTs unclear. Other proposed formation mechanisms, such as removal of dark dust, exposure of a bright underlying substrate, a compaction mechanism by the downdraft of dust devils, might also lead to tracks having higher reflective surfaces. The lifetimes of bright DDTs seem to be sub-annual, similar to the dark continuous DDTs on Mars and Earth. Future in situ and orbital martian studies are needed to understand the formation mechanism of bright DDTs on Mars.

In general, the suggested formation mechanisms of different DDT types are all based on only a few in situ studies. Therefore, other formation mechanisms leading to the same morphologies can not be excluded. In addition, it is also plausible that two different processes are simultaneously responsible for creating tracks, e.g., removal of dust and redistribution of sand-sized material.

On Earth, observed DDTs are limited to semi-arid to arid regions and have been reported in the Sahara desert, arid regions in northwestern China, and the coastal Peruvian desert. On Mars, they occur globally (except on the permanent polar caps) and can be found at all topographic elevations. They are formed most frequently during spring and summer, when insolation is around its maximum, triggering dust devil formation (see also Rafkin et al. 2016, this issue). Mapped DDT densities in the southern hemisphere (0.6 DDTs/km^2) are about 10 times higher than those in the northern hemisphere (0.06 DDTs/km^2), which is probably mainly related to Mars's orbital eccentricity in which the southern hemisphere receives about 40% stronger insolation during southern summer than the northern hemisphere during northern summer. Regionally, large variations in DDT distributions and densities occur on Mars and there exists no relationship between observed active dust devils and DDT frequencies, implying that DDT formation is strongly controlled by surface properties, e.g. dust cover thickness. Currently, there exists no distribution study in which all three DDT types have been separately mapped on Mars. However, future studies mapping the three different types separately and relating their location to thermophysical surface properties may give insights into the formation mechanism of DDTs on Mars, especially for the less common dark cycloidal and bright DDTs. In general, the automatic detection of DDTs from satellite imagery could help to minimize time consuming mapping procedures and include larger data sets.

DDTs can indirectly be used as indicators for several processes. Obviously, their frequent occurrence and relatively long visibility on the surface, in contrast to direct observations of active dust devils trough satellite imagery snapshots (see Fenton et al. 2016, this issue), have been used to infer global dust devil activity and quantify how much dust devils contribute to the global dust entrainment into Mars's atmosphere. Although the derived calculations can be used as a first-order estimate, several uncertainties remain to be resolved in the future to constrain the contribution of dust devils in replenishing the background dust opacity on Mars from DDTs. Using DDTs as a proxy for dust devil frequency is problematic because the formation of DDTs and therefore the DDT spatial density in an area is strongly controlled by surface properties, such as dust availability and albedo contrast with the substrate, the intensity of dust devils, and the horizontal ground speeds of dust devils, which are related to the ambient wind fields. These parameters vary on local and regional scales and likely represent the main reasons for the large regional differences in DDT frequencies and proportions of how many active dust devils are able to leave tracks. However, future studies could decompose the individual parameters that influence DDT frequencies on local to global scales, hence providing better knowledge about dust devil activity as well as their contribution to dust entrainment on Mars (see also Klose et al. 2016, this issue). However, while DDTs can not yet be used as an accurate proxy for dust devil frequency, DDTs can be used as good proxies for inferring minimum dust devil durations (lifetimes), wind directions (from the morphology of dark cycloidal DDTs, ambient wind directions from DDT orientations with the help of climate models, and predicting solar panel dust clearing recurrence intervals, which is important for future Mars landing missions that depend on power from solar arrays.

Finally, DDT formation mechanisms may reveal new insights about other active processes on Mars related to albedo changes. Mass wasting and aeolian processes with dark or bright features, such as slope streaks (e.g., Sullivan et al. 2001; Schorghofer and King 2011), wind streaks (e.g., Thomas et al 1981; Geissler et al. 2008), or Recurrent Slope Linea (RSL) (e.g., McEwen et al. 2011; Ojha et al. 2015), may share the same formation mechanisms. Currently, there are no comprehensive studies comparing such features with each other or quantifying their similarities or differences, such as albedo contrasts. However, future comprehensive analog studies between these different albedo contrast features on Mars may help improve our knowledge about the different formation processes and constrain their formation mechanisms.

References

M. Balme, R. Greeley, Dust devils on Earth and Mars. Rev. Geophys. **44**, RG3003 (2006), doi:10.1029/2005RG000188.

M. R. Balme, P. L. Whelley, R. Greeley, Mars: Dust devil track survey in Argyre Planitia and Hellas Basin. J. Geophys. Res. **108**, 5086 (2003), doi:10.1029/2003JE002096.

M. R. Balme, A. Pathare, S. M. Metzger, M. C. Towner, S. R. Lewis, A. Spiga, L. Fenton, N. O. Renno, H. M. Elliott, F. A. Saca, T. Michaels, P. Russell, J. Verdasca, Field measurements of horizontal forward motion velocities of terrestrial dust devils: Towards a proxy for ambient winds on Mars and Earth. Icarus. 221, 632–645 (2012).

L. Bandeira, J. S. Marques, J. Saraiva, P. Pina, Automated Detection of Martian Dune Fields. IEEE Geoscience and Remote Sensing Letters. **8**, 626-630 (2011).

Bennett, K. A., Fenton, L., Bell, J. F. III. (2016) The albedo of martian dunes: Insights into aeolian activity and dust devil formation, in review at Aeolian Research.

J. A. Berger, M. E. Schmidt, R. Gellert, J. L. Campbell, P. L. King, R. L. Flemming, D. W. Ming, B. C. Clark, I. Pradler, S. J. V Vanbommel, M. E. Minitti, A. G. Fairén, N. I. Boyd, L. M. Thompson, G. M. Perrett, B. E. Elliott, E. Desouza, A global Mars dust composition refined by the Alpha-Particle X-ray Spectrometer in Gale Crater. Geophys. Res. Lett. 43, 67–75 (2016).

N. T. Bridges, M. E. Banks, R. A. Beyer, F. C. Chuang, E. Z. Noe Dobrea, K. E. Herkenhoff, L. P. Keszthelyi, K. E. Fishbaugh, A. S. McEwen, T. I. Michaels, Aeolian bedforms, yardangs, and indurated surfaces in the Tharsis Montes as seen by the HiRISE Camera: Evidence for dust aggregates. *Icarus*. **205**, 165–182 (2010).

N. T. Bridges, M. C. Bourke, P. E. Geissler, M. E. Banks, C. Colon, S. Diniega, M. P. Golombek, C. J. Hansen, S. Mattson, A. S. Mcewen, M. T. Mellon, N. Stantzos, B. J. Thomson, Planet-wide sand motion on Mars. Geology (2011), doi:10.1130/G32373.1.

F. J. Calef, V. L. Sharpton, Enigmatic linear features in the Northern Hemisphere of Mars: Their formation process. Geophys. Res. Lett. **32**, L24202 (2005), doi:10.1029/2005GL023868.

B. A. Cantor, K. M. Kanak, K. S. Edgett, Mars Orbiter Camera observations of Martian dust devils and their tracks (September 1997 to January 2006) and evaluation of theoretical vortex models. J. Geophys. Res. **111**, E12002 (2006), doi:10.1029/2006JE002700.

J. J. Carroll, J. A. Ryan, Atmospheric vorticity and dust devil rotation. J. Geophys. Res. 75, 5179–5184 (1970).

D. S. Choi, C. M. Dundas, Measurements of Martian Dust Devil Winds with HiRISE. Geophys. Res. Lett. 38 (2011), doi:10.1029/2011GL049806.

Christensen PR (1988) Global albedo variations on Mars - Implications for active aeolian transport, deposition, and erosion. J Geophys Res 93:7611–7624. doi: 10.1029/JB093iB07p07611

Christensen, P.R., Bandfield, J.L., Hamilton, V.E., Ruff, S.W., Kieffer, H.H., Titus, T.N., Malin, M.C., Morris, R. V., Lane, M.D., Clark, R.L., Jakosky, B.M., Mellon, M.T., Pearl, J.C., Conrath, B.J., Smith, M.D., Clancy, R.T., Kuzmin, R.O., Roush, T., Mehall, G.L., Gorelick, N., Bender, K., Murray, K., Dason, S., Greene, E., Silverman, S., Greenfield, M., 2001. Mars Global Surveyor Thermal Emission Spectrometer experiment: Investigation description and surface science results. J. Geophys. Res. 106, 23823–23871.

R. N. Clark T.L. Roush, Reflectance spectroscopy: Quantitative analysis techniques for remote sensing applications, *J. Geophys. Res.*, **89,** 6329- 6340, (1984).

Crisp, D., Pathare, A., Ewell, R.C., 2004. The performance of gallium arsenide/germanium solar cells at the Martian surface. Acta Astronaut. 54, 83–101.

G. E. Cushing, T. N. Titus, P. R. Christensen, THEMIS VIS and IR observations of a high-altitude Martian dust devil. Geophys. Res. Lett. **32** (2005), doi:10.1029/2005GL024478.

J. A. Cutts, R. S. U. Smith, Eolian deposits and dunes on Mars. *J. Geophys. Res.* **78**, 4139–4154 (1973).

Davies-Jones, R. P. (1986), Tornado dynamics, in Thunderstorm Morphology and Dynamics, Chap. 10, pp. 197 – 388, Univ. of Okla. Press, Norman.

N. B. Drake, L. K. Tamppari, R. D. Baker, B. A. Cantor, A. S. Hale, Dust devil tracks and wind streaks in the North Polar Region of Mars: A study of the 2007 Phoenix Mars Lander Sites. Geophys. Res. Lett. **33**, L19S02 (2006), doi:10.1029/2006GL026270.

K. S. Edgett, M. C. Malin, Martian Dust Raising and Surface Albedo Controls: Thin, Dark (and Sometimes Bright) Streaks and Dust Devils in MGS MOC High Resolution Images, in *Lunar and Planetary Science Conference XXXI* (2000), Abstract #1073.

L. Fenton, D. Reiss, M. Lemmon, B. Marticorena, S. Lewis, B. Cantor, Orbital Observations of Dust Lofted by Daytime Convective Turbulence, *Space Sci. Rev.*, 2016.

L. K. Fenton, P. E. Geissler, R. M. Haberle, Global warming and climate forcing by recent albedo changes on Mars. Nature **446**, 646–649 (2007), doi:10.1038/nature05718.

Fenton, L. K., A. D. Toigo, and M. I. Richardson (2005), Aeolian processes in Proctor Crater on Mars: Mesoscale modeling of dune-forming winds, *J. Geophys. Res.*, *110*(E06005), doi:10.1029/2004JE002309.

Fenton, L. K., J. L. Bandfield, and A. W. Ward (2003), Aeolian processes in Proctor Crater on Mars: Sedimentary history as analyzed from multiple data sets, J. Geophys. Res., 108(E12, 5129), doi:10.1029/2002JE002015.

J. A. Fisher, M. I. Richardson, C. E. Newman, M. A. Szwast, C. Graf, S. Basu, S. P. Ewald, A. D. Toigo, R. J. Wilson, A survey of Martian dust devil activity using Mars Global Surveyor Mars Orbiter Camera images. J. Geophys. Res. **110**, E03004 (2005), doi:10.1029/2003JE002165.

D. E. Fitzjarrald, A Field investigation of Dust Devils. *J. Appl. Meteorol.* **12**, 808–813 (1973).

T. T. Fujita, D. L. Bradbury, C. F. van Thullenar, Palm Sundy Tornadoes of April 11, 1965. Mon. Wea. Rev. 98, 29-69 (1970).

T. T. Fujita, Proposed Mechanism of Suction Spots accompanied by Tornadoes. Preprints of papers presented at the Seventh Conference on Severe Local Storms. October 5-7, 1971, Kansas City, Mo., 208-213, (1971).

T. T. Fujita, Jumbo Tornado Outbreak of 3 April 1974. Weatherwise 27, 116-126 (1974).

P. J. Gierasch, R. M. Goody, A model of a martian great dust storm. J. Atmos. Sci. 30, 169–179 (1973).

Geissler, P. E., Fenton, L. K., Enga, M.-T., Mukherjee, P. (2016) Orbital monitoring of martian surface changes, in press at Icarus, doi:10.1016/j.icarus.2016.05.023.

P. E. Geissler, Three decades of Martian surface changes. J. Geophys. Res. **110**, E02001 (2005), doi:10.1029/2004JE002345.

P. E. Geissler, R. Sullivan, M. Golombek, J. R. Johnson, K. Herkenhoff, N. Bridges, a. Vaughan, J. Maki, T. Parker, J. Bell, Gone with the wind: Eolian erasure of the Mars Rover tracks. J. Geophys. Res. 115, 1–17 (2010).

P. E. Geissler, J. R. Johnson, R. Sullivan, K. Herkenhoff, D. Mittlefehldt, R. Fergason, D. Ming, R. Morris, S. Squyres, L. Soderblom, M. Golombek, First in situ investigation of a dark wind streak on Mars. J. Geophys. Res. 113, 1–16 (2008).

W. Goetz, P. Bertelsen, C. S. Binau, H. P. Gunnlaugsson, S. F. Hviid, K. M. Kinch, D. E. Madsen, M. B. Madsen, M. Olsen, R. Gellert, G. Klingelhöfer, D. W. Ming, R. V Morris, R. Rieder, D. S. Rodionov, P. A. de Souza, C. Schröder, S. W. Squyres, T. Wdowiak, A. Yen, Indication of drier periods on Mars from the chemistry and mineralogy of atmospheric dust. Nature. 436, 62–65 (2005).

J. A. Grant, P. H. Schultz, Possible tornado-like tracks on Mars. Science **237**, 883–885 (1987).

R. Greeley, J. D. Iversen, Wind as a geological process on Earth, Mars, Venus, and Titan. Cambridge University Press, New York, p. 333.

R. Greeley, D. A. Waller, N. A. Cabrol, G. A. Landis, M. T. Lemmon, L. D. V. Neakrase, M. Pendeleton Hoffer, S. D. Thompson, P. L. Whelley, Gusev crater, Mars: Observations of three dust devil seasons. J. Geophys. Res. **115**, E00F02 (2010), doi:10.1029/2010JE003608.

R. Greeley, R. Arvidson, J. F. Bell III, P. Christensen, D. Foley, A. Haldemann, R. O. Kuzmin, G. A. Landis, L. D. V. Neakrase, G. Neukum, S. W. Squyres, R. Sullivan, S. D. Thompson, P. L. Whelley, D. Williams, Martian variable features: New insight from the Mars Express Orbiter and the Mars Exploration Rover Spirit. J. Geophys. Res. **110**, E06002 (2005), doi:10.1029/2005JE002403.

R. Greeley, R. E. Arvidson, P. W. Barlett, D. Blaney, N. A. Cabrol, P. R. Christensen, R. L. Fergason, M. P. Golombek, G. A. Landis, M. T. Lemmon, S. M. McLennan, J. N. Maki, T. Michaels, J. E. Moersch, L. D. V. Neakrase, S. C. R. Rafkin, L. Richter, S. W. Squyres, P. a. de Souza, R. J. Sullivan, S. D. Thompson, P. L. Whelley, Gusev crater: Wind-related features and processes observed by the Mars Exploration Rover Spirit. J. Geophys. Res. **111**, E02S09 (2006a), doi:10.1029/2005JE002491.

R. Greeley, P. L. Whelley, R. E. Arvidson, N. A. Cabrol, D. J. Foley, B. J. Franklin, P. G. Geissler, M. P. Golombek, R. O. Kuzmin, G. A. Landis, M. T. Lemmon, L. D. V. Neakrase, S. W. Squyres, S. D. Thompson, Active dust devils in Gusev crater, Mars: Observations from the Mars Exploration Rover Spirit. J. Geophys. Res. **111**, E12S09 (2006b), doi:10.1029/2006JE002743.

R. Greeley, P. L. Whelley, L. D. V. Neakrase, Martian dust devils: Directions of movement inferred from their tracks. Geophys. Res. Lett. **31**, L24702 (2004), doi:10.1029/2004GL021599.

R. Greeley, M. R. Balme, J. D. Iversen, S. M. Metzger, R. Mickelson, J. Phoreman, B. White, Martian dust devils: Laboratory simulations of particle threshold. J. Geophys. Res. 108 (2003), doi:10.1029/2002JE001987.

K. Gwinner, R. Jaumann, E. Hauber, H. Hoffmann, C. Heipke, J. Oberst, G. Neukum, V. Ansan, J. Bostelmann, A. Dumke, S. Elgner, G. Erkeling, F. Fueten, H. Hiesinger, N. M. Hoekzema, E. Kersten, D. Loizeau, K.-D. Matz, P. C. McGuire, V. Mertens, G. Michael, A. Pasewaldt, P. Pinet, F. Preusker, D. Reiss, T. Roatsch, R. Schmidt, F. Scholten, M. Spiegel, R. Stesky, D. Tirsch, S. van Gasselt, S. Walter, M. Wählisch, K. Willner, The High Resolution Stereo Camera (HRSC) of Mars Express and its Approach to Science Analysis and Mapping for Mars and its Satellites. Planet. Space Sci. 126, 93–138 (2016).

Haberle RM, Kahre MA, Murphy JR, et al (2006) Role of dust devils and orbital precession in closing the Martian dust cycle. Geophys Res Lett 33:1–4. doi: 10.1029/2006GL026188.

P. K. Haff, B. T. Werner, Dynamical processes on desert pavements and the healing of surfical disturbances. Quat. Res. 45, 38 – 46 (1996).

B. Hapke, Bidirectional reflectance spectroscopy 1. Theory, J. Geophys. Res. 86, 3039-3054 (1981)

B. Hapke, Introduction to the Theory of reflectance and Emittance Spectroscopy, Cambridge University Press, New York (1993).

C. L. L. Hendriks, Constrained and dimensionality-independent Path Openings. IEEE Transactions on Image Processing. **19**, 1587-1595 (2010).

Herkenhoff, K.E. et al., 2004. Textures of the soils and rocks at Gusev crater from Spirit's Microscopic Imager. Science 305, 824–826.

Herkenhoff, K.E. et al., 2006. Overview of the Microscopic Imager investigation during Spirit's first 450 sols in Gusev crater. J. Geophys. Res. 110, E02S04. doi:10.1029/2005JE002574.

R. Hesse, Short-lived and long-lived dust devil tracks in the coastal desert of southern Peru. Aeolian Res. **5**, 101–106 (2012), doi:10.1016/j.aeolia.2011.10.003.

Hoffer, M.P., Greeley, R., 2010. Bright tracks on Mars: Alternate dust devil tracks. Lunar Planet. Sci. 41. Abstract 2713.

C. Holstein-Rathlou, H. P. Gunnlaugsson, J. P. Merrison, K. M. Bean, B. a. Cantor, J. a. Davis, R. Davy, N. B. Drake, M. D. Ellehoj, W. Goetz, S. F. Hviid, C. F. Lange, S. E. Larsen, M. T. Lemmon, M. B. Madsen, M. Malin, J. E. Moores, P. Nørnberg, P. Smith, L. K. Tamppari, P. a. Taylor, Winds at the Phoenix landing site. J. Geophys. Res. 115, E00E18 (2010).

J. D. Iversen, B. R. White, Saltation threshold on Earth, Mars and Venus. Sedimentology. 29, 111–119 (1982).

Kahre MA, Murphy JR, Haberle RM (2006) Modeling the Martian dust cycle and surface dust reservoirs with the NASA Ames general circulation model. J Geophys Res 111:1–25. doi: 10.1029/2005JE002588

M. Klose, et al., Space Sci. Rev., 2016, in press.

J. F. Kok, E. J. R. Parteli, T. I. Michaels, D. B. Karam, The physics of wind-blown sand and dust. Reports Prog. Phys. 75, 72 (2012).

Landis, G.A., Jenkins, P.P., 2000. Measurement of the settling rate of atmospheric dust on Mars by the MAE instrument on Mars Pathfinder. J. Geophys. Res. 105, 1855–1857.

Lemmon, M.T., Wolff, M.J., Smith, M.D., Clancy, R.T., Banfield, D., Landis, G.A., Ghosh, A., Smith, P.H., Spanovich, N., Whitney, B., Whelley, P., Greeley, R., Thompson, S., Bell, J.F., Squyres, S.W., 2004. Atmospheric imaging results from the Mars Exploration Rovers: Spirit and Opportunity. Science 306, 1753–6.

D. C. Lewellen, W. S. Lewellen, and J. Xia, 2000: The Influence of a Local Swirl Ratio on Tornado Intensification near the Surface. *J. Atmos. Sci.*,**57**, 527–544.

D. C. Lewellen and W. S. Lewellen, 2007a: Near-Surface Intensification of Tornado Vortices. *J. Atmos. Sci.*, **64**, 2176–2194.

D. C. Lewellen and W. S. Lewellen, 2007b: Near-Surface Vortex Intensification through Corner Flow Collapse. *J. Atmos. Sci.*, **64**, 2195–2209.

D. C. Lewellen, Baiyun Gong, and W. S. Lewellen, 2008: Effects of Finescale Debris on Near-Surface Tornado Dynamics. *J. Atmos. Sci.*, **65**, 3247–3262.

D. C. Lewellen and M. I. Zimmerman, 2008: Using tornado surface marks to help decipher near-ground wind fields, *24th Conf. Severe Local Storms*.

R. D. Lorenz, M. R. Balme, G. Zhaolin, H. Kahanpää, M. Klose, M. V. Kurgansky, M. R. Patel, D. Reiss, A. P. Rossi, A. Spiga, T. Takemi, W. Wei, History and Applications of Dust Devil Studies, Space Sci. Rev., 2016.

R. D. Lorenz, B. Jackson, Dust Devil Populations and Statistics, Space Sci. Rev., 2016.

R. D. Lorenz, The Longevity and Aspect Ratio of Dust Devils: Effects on Detection Efficiencies and Comparison of Landed and Orbital Imaging at Mars. Icarus. **226**, 964–970 (2013), doi:10.1016/j.icarus.2013.06.031.

Lorenz, R. D., Irregular Dust Devil Pressure Drops on Earth and Mars: Effect of Cycloidal Tracks, Planetary and Space Science, 76, 96-103, 2013b.

R. D. Lorenz, On the Statistical Distribution of Dust Devil Diameters. Icarus. **215**, 381–390 (2011), doi:10.1016/j.icarus.2011.06.005.

R. D. Lorenz, Power law of dust devil diameters on Mars and Earth. Icarus. **203**, 683–684 (2009), doi:10.1016/j.icarus.2009.06.029.

R. D. Lorenz, D. Reiss, Solar panel clearing events, dust devil tracks, and in-situ vortex detections on Mars. Icarus. **248**, 162–164 (2015), doi:10.1016/j.icarus.2014.10.034.

Lorenz, R. D., 2016. Heuristic Estimation of Dust Devil Vortex Parameters and Trajectories from Single-Station Meteorological Data: Application to InSight at Mars, Icarus, 271, 326-337.

L. J. Maher, Geology education by lightplane. The AOPA Pilot **11**(1), 60-65 (1968).

M. C. Malin, K. S. Edgett, Mars Global Surveyor Mars orbiter Camera: Interplanetary cruise through primary mission. J. Geophys. Res. **106**, 23429–23570 (2001).

Markiewicz, W.J., Sablotny, R.M., Keller, H.U., Thomas, N., Titov, D., Smith, P.H., 1999. Optical properties of the Martian aerosols as derived from Imager for Mars Pathfinder midday sky brightness data. Journal of Geophysical Research 104, 9009–9017.

A. S. McEwen, L. Ojha, C. M. Dundas, S. S. Mattson, S. Byrne, J. J. Wray, S. C. Cull, S. L. Murchie, N. Thomas, V. C. Gulick, Seasonal Flows on Warm Martian Slopes. Science (80-.). 333, 740–743 (2011).

Mellon, M. T., K. A. Kretke, M. D. Smith, and S. M. Pelkey, A global map of thermal inertia from Mars Global Surveyor Mapping Mission, Lunar Planet. Sci. [CDROM], XXXIII, Abstract 1416, 2002.

S. M. Metzger, M. R. Balme, M. C. Towner, B. J. Bos, T. J. Ringrose, M. R. Patel, In situ measurements of particle load and transport in dust devils. *Icarus*. **214**, 766–772 (2011).

S. M. Metzger, Dust devils as aeolian transport mechanisms in southern Nevada and in the Mars Pathfinder landing site, PhD thesis, Univ. of Nev., Reno, p. 208 (1999).

T. I. Michaels, Numerical modeling of Mars dust devils: Albedo track generation. Geophys. Res. Lett. **33**, L19S08 (2006), doi:10.1029/2006GL026268.

F. M. Neubauer, Thermal convection in the Martian atmosphere. *J. Geophys. Res.* **71**, 2419–2426 (1966).

L. D. V. Neakrase, A Laboratory Study of Sediment Flux within Dust Devils on Earth and Mars, Arizona State University, ProQuest, 184 pages, (2009).

L. D. V. Neakrase, J. McHone, P. L. Whelley, R. Greeley, Saharan Dust Devil Tracks: Mars Analog Field Study Areas. *Geol. Soc. Am. Abstr.* **40**, 262 (2008).

L. D. V. Neakrase, J. McHone, P. L. Whelley, R. Greeley, Terrestrial analogs to Mars: East-central saharan dust devil tracks, in *43rd Lunar and Planetary Science Conference* (2012), Abstract #2009.

Ojha, M. B. Wilhelm, S. L. Murchie, A. S. Mcewen, J. J. Wray, J. Hanley, M. Massé, M. Chojnacki, Spectral evidence for hydrated salts in recurring slope lineae on Mars. Nat. Geosci. 8, 829–832 (2015).

J. Ormö, G. Komatsu, Mars Orbiter Camera observation of linear and curvilinear features in the Hellas basin: Indications for multiple processes of formation. J. Geophys. Res. **108**, 5059 (2003), doi:10.1029/2002JE001980.

N. Otsu, A threshold selection method from gray-level histograms. IEEE T. Syst. Man. Cyb. **9**, 62-66 (1979).

A. V. Pathare, M. R. Balme, S. M. Metzger, A. Spiga, M. C. Towner, N. O. Renno, F. Saca, Assessing the power law hypothesis for the size–frequency distribution of terrestrial and martian dust devils. *Icarus*. **209**, 851–853 (2010).

Pollack, J.B., Ockert-Bell, M.E., Shepard, M.K., 1995. Viking Lander image analysis of Martian atmospheric dust. Journal of Geophysical Research 100, 5235–5250.

N. E. Prosser, Aerial Photographs of a Tornado Path in Nebraska, May 5, 1964. Mon. Wea. Rev. 92, 593-598.

Putzig, N. E., M. T. Mellon, K. A. Kretke, and R. E. Arvidson, Global thermal inertia and surface properties of Mars from the MGS mapping mission, Icarus 173, 325-341, 2005.

D. Reiss, A. Spiga, G. Erkeling, The horizontal motion of dust devils on Mars derived from CRISM and CTX / HiRISE observations. Icarus. **227**, 8–20 (2014a), doi:10.1016/j.icarus.2013.08.028.

D. Reiss, N. M. Hoekzema, O. J. Stenzel, Dust deflation by dust devils on Mars derived from optical depth measurements using the shadow method in HiRISE images. Planet. Space Sci. **93-94**, 54–64 (2014b), doi:10.1016/j.pss.2014.01.016.

D. Reiss, J. Raack, A. P. Rossi, G. Di Achille, H. Hiesinger, First in-situ analysis of dust devil tracks on Earth and their comparison with tracks on Mars. Geophys. Res. Lett. **37**, L14203 (2010), doi:10.1029/2010GL044016.

D. Reiss, M. Zanetti, G. Neukum, Multitemporal observations of identical active dust devils on Mars with the High Resolution Stereo Camera (HRSC) and Mars Orbiter Camera (MOC). Icarus. **215**, 358–369 (2011).

D. Reiss, J. Raack, H. Hiesinger, Bright dust devil tracks on Earth: Implications for their formation on Mars. Icarus. **211**, 917–920 (2011a), doi:10.1016/j.icarus.2010.09.009.

D. Reiss, J. Raack, A. Maturilli, A. P. Rossi, G. Erkeling, Dust devil tracks in the Turpan Depression desert (China): Implications for their formation on Mars, in *43rd Lunar and Planetary Science Conference* (2012), Abstract #2227.

D. Reiss, J. Raack, G. G. Ori, K. Taj-Eddine, In situ analysis of dust devil tracks in southern Morocco: Comparison with other terrestrial and martian tracks, EPSC 2012, Abstract #EPSC2012-389, (2012b).

D. Reiss, R. D. Lorenz, Dust Devil Track Survey at Elysium Planitia, Mars: Implications for the InSight landing sites. *Icarus*. **266**, 315–330 (2016).

D. Reiss, M. I. Zimmerman, D. C. Lewellen, Formation of cycloidal dust devil tracks by redeposition of coarse sands in southern Peru: Implications for Mars. Earth Planet. Sci. Lett. **383**, 7–15 (2013), doi:10.1016/j.epsl.2013.09.033.

D. Reiss, A. P. Rossi, Seasonal Dust Devil Track Observations on Earth and Mars: Relationships to Atmospheric Dust Opacity. Lunar and Planetary Science Conference, Vol. 42, #2186 (2011).

D. Reiss, Morphology, formation and distribution of dust devil tracks on Mars: Insights from terrestrial analogs, Lunar and Planetary Science Conference, Vol. 45, #2011 (2014).

Rennó NO, Burkett ML, Larkin MP (1998) A simple thermodynamical theory for dust devils. J Atmos Sci 55:3244–3252.

R. Rieder, T. Economou, H. Wänke, A. Turkevich, J. Crisp, J. Brückner, G. Dreibus, H. J. McSween Jr., The Chemical Composition of Martian Soil and Rocks Returned by the Mobile Alpha Proton X-ray Spectrometer: Preliminary Results from the X-ray Mode. Science 278, 1771–1774 (1997).

A. P. Rossi, L. Marinangeli, The first terrestrial analogue to Martian dust devil tracks found in Ténéré Desert, Niger. Geophys. Res. Lett. **31**, L06702 (2004), doi:10.1029/2004GL019428.

S. W. Ruff, P. R. Christensen, Bright and dark regions on Mars: Particle size and mineralogical characteristics based on Thermal Emission Spectrometer data. J. Geophys. Res. 107, 5217 (2002).

J. A. Ryan, Notes on the Martian yellow clouds. *J. Geophys. Res.* **69**, 3759–3770 (1964).

J. A. Ryan, J. J. Carroll, Dust devil wind velocities: Mature state. *J. Geophys. Res.* **75**, 531–541 (1970).

J. A. Ryan, R. D. Lucich, Possible dust devils, vortices on Mars. *J. Geophys. Res.* **88**, 11005–11011 (1983).

C. Sagan, J. Veverka, P. Gierasch, Observational consequences of Martian wind regimes. *Icarus*. **15**, 253–278 (1971).

C. Sagan, J. Veverka, P. Fox, R. Dubisch, J. Lederberg, E. Levinthal, L. Quam, R. Tucker, J. B. Pollack, B. A. Smith, Variable features on Mars: Preliminary mariner 9 television results. *Icarus*. **17**, 346–372 (1972).

Sagan, C., et al. (1973), Variable features in Mars: 2. Mariner 9 global results, J. Geophys. Res., 78, 4163–4196.

N. Schorghofer, C. M. King, Sporadic formation of slope streaks on Mars. Icarus. 216, 159–168 (2011).

Silvestro, S., L. K. Fenton, D. A. Vaz, N. T. Bridges, and G. G. Ori (2010), Ripple migration and dune activity on Mars: Evidence for dynamic wind processes, Geophys. Res. Lett., 37, L20203, doi:10.1029/2010GL044743.

P. C. Sinclair, A quantitative analysis of the dust devil, PhD thesis, University of Arizona, 292 p (1966).

P. C. Sinclair, General characteristics of dust devils. J. Appl. Meteorol. 8, 32–45 (1969).

P. C. Sinclair, The Lower Structure of Dust Devils. *J. Atmos. Sci.* **30**, 1599–1619 (1973).

Smith MD (2004) Interannual variability in TES atmospheric observations of Mars during 1999–2003. Icarus 167:148–165. doi: 10.1016/j.icarus.2003.09.010

J. T. Snow, T. M. McClelland, Dust Devils at White Sands Missile Range, New Mexico 1. Temporal and Spatial Distributions. *J. Geophys. Res.* **95**, 13707–13721 (1990).

Spiga, A. et al., Large-Eddy Simulations of dust devils and convective vortices, Space Science Reviews, 2016, in press.

C. Stanzel, M. Pätzold, D. A. Williams, P. L. Whelley, R. Greeley, G. Neukum, HRSC Co-Investigator Team, Dust devil speeds, directions of motion and general characteristics observed by the Mars Express High Resolution Stereo Camera. Icarus. **197**, 39–51 (2008), doi:10.1016/j.icarus.2008.04.017.

T. Statella, P. Pina, E. A. da Silva, A Study on Automatic Methods Based on Mathematical Morphology for Martian Dust Devil Tracks Detection. Lect. Notes Comput. Sci. **7042**, 533–540 (2011).

T. Statella, P. Pina, E. A. da Silva, Automated determination of the orientation of dust devil tracks in mars orbiter images. Adv. Sp. Res. **53**, 1822–1833 (2014), doi:10.1016/j.asr.2013.05.012.

T. Statella, P. Pina, E. A. da Silva, Image Processing Algorithm for the Identification of Martian Dust Devil Tracks in MOC and HiRISE Images. Planet. Space Sci. **70**, 46–58 (2012), doi:10.1016/j.pss.2012.06.003.

T. Statella, P. Pina, E. A. Da Silva, Extensive computation of albedo contrast between martian dust devil tracks and their neighboring regions. Icarus. **250**, 43–52 (2015), doi:10.1016/j.icarus.2014.11.023.

R. Sullivan, P. Thomas, J. Veverka, M. Malin, K. S. Edgett, Mass movement slope streaks imaged by the Mars Orbiter Camera. J. Geophys. Res. 106, 23607–23633 (2001).

R. Sullivan, R. Arvidson, J. F. Bell, R. Gellert, M. Golombek, R. Greeley, K. Herkenhoff, J. Johnson, S. Thompson, P. Whelley, J. Wray, Wind-driven particle mobility on Mars: Insights from Mars Exploration Rover observations at “El Dorado” and surroundings at Gusev Crater. J. Geophys. Res. 113, E06S07 (2008).

Szwast MA, Richardson MI, Vasavada AR (2006) Surface dust redistribution on Mars as observed by the Mars Global Surveyor and Viking orbiters. J Geophys Res 111:E11008. doi: 10.1029/2005JE002485.

P. Thomas, J. Veverka, S. Lee, A. Bloom, Classification of wind streaks on Mars. Icarus. 45, 124–153 (1981).

P. Thomas, P. J. Gierasch, Dust devils on Mars. *Science* **230**, 175–177 (1985).

Tomasko, M., Doose, L., Lemmon, M., Smith, P., Wegryn, E., 1999. Properties of dust in the Martian atmosphere from the Imager on Mars Pathfinder. Journal of Geophysical Research 104, 8987-9007.

Van Tassel, E. L., The North Platte Valley Tornado Outbreak of june 27, 1955. Mon. Wea. Rev. 83, 255-264 (1955).

A. F. Vaughan, J. R. Johnson, K. E. Herkenhoff, R. Sullivan, G. A. Landis, W. Goetz, M. B. Madsen, Pancam and Microscopic Imager observations of dust on the Spirit Rover: Cleaning events, spectral properties, and aggregates. Mars J. 5, 129–145 (2010).

C. A. Verba, P. E. Geissler, T. N. Titus, D. A. Waller, Observations from High Resolution Imaging Science Experiment (HiRISE): Martian dust devils in Gusev and Russell craters. J. Geophys. Res. **115**, E09002 (2010), doi:10.1029/2009JE003498.

J. Veverka, Variable Features on Mars. VII. Dark Filamentary Markings on Mars. Icarus **27**, 495–502 (1976).

J. Veverka, Variable features on Mars V: Evidence for crater streaks produced by wind erosion. Icarus. 25, 595–601 (1975).

E. Wells, J. Veverka, P. Thomas, Mars: Experimental study of albedo changes caused by dust fallout. Icarus. 58, 331–338 (1984).

P. L. Whelley, R. Greeley, Latitudinal dependency in dust devil activity on Mars. J. Geophys. Res. **111**, E10003 (2006), doi:10.1029/2006JE002677.

P. L. Whelley, R. Greeley, The distribution of dust devil activity on Mars. J. Geophys. Res. **113**, E07002 (2008), doi:10.1029/2007JE002966.

Wolff, M.J. and 12 colleagues, 2006. Constraints on dust aerosols from the Mars Exploration Rovers using MGS overflights and Mini-TES. J. Geophys. Res., 111, E12S17, doi:10.1029/2006JE002786.

A. S. Yen, R. Gellert, C. Schröder, R. V Morris, J. F. Bell, A. T. Knudson, B. C. Clark, D. W. Ming, J. A. Crisp, R. E. Arvidson, D. Blaney, J. Brückner, P. R. Christensen, D. J. DesMarais, P. A. de Souza, T. E. Economou, A. Ghosh, B. C. Hahn, K. E. Herkenhoff, L. a Haskin, J. A. Hurowitz, B. L. Joliff, J. R. Johnson, G. Klingelhöfer, M. B. Madsen, S. M. McLennan, H. Y. McSween, L. Richter, R. Rieder, D. Rodionov, L. Soderblom, S. W. Squyres, N. J. Tosca, A. Wang, M. Wyatt, J. Zipfel, An integrated view of the chemistry and mineralogy of martian soils. Nature. 436, 49–54 (2005).

M. I. Zimmerman and D. C. Lewellen, 2010: Taxonomy and analysis of tornado surface marks, *25th Conf. Severe Local Storms*.

Zomer RJ, Trabucco A, Bossio DA, van Straaten O, Verchot LV, 2008. Climate Change Mitigation: A Spatial Analysis of Global Land Suitability for Clean Development Mechanism Afforestation and Reforestation. Agric. Ecosystems and Envir. 126: 67-80.

Zomer RJ, Bossio DA, Trabucco A, Yuanjie L, Gupta DC & Singh VP, 2007. Trees and Water: Smallholder Agroforestry on Irrigated Lands in Northern India. Colombo, Sri Lanka: International Water Management Institute. pp 45. (IWMI Research Report 122).

Zurek, R. W., J. R. Barnes, R. M. Haberle, J. B. Pollack, J. E. Tillman, and C. B. Leovy, Dynamics of the atmosphere of Mars, in Mars, edited by H. H. Kieffer et al., pp. 799–817, Univ. of Ariz. Press, Tucson, 1992.